CTF3 DESIGN REPORT

Preliminary Phase

D. Allard, B. Bartholome, J.P. Bertuzzi, R. Bonzano, R. Bossart, H. Braun, E. Bravin, J. Borburgh, J. Buttkus, E. Chazarenc, V. Chohan, J.J. Cloye, R. Corsini, G. Coudert, M. Damiani, S. Deghaye, J.P. Delahaye, F. Di Maio, T. Dobers, P. Dubief, B. Dupuy, L.Durieu, A. Ferrari, G. Geschonke, J. Hansen, H. Hellgren, M. Hourican, M. Lamidon, T. Lefevre, J.H. Lewis, J. Lindroos, E. Mahner, G. McMonagle, J. Monteiro, J. Mourier, P. Odier, T. Otto, P. Pearce, R. Pittin, M. Poehler, J-P. Potier, U. Raich, M. Rettig, L. Rinolfi, T. Risselada, R. Riva, G. Rossat, P. Royer, L. Sermeus, K. Setas, G. Simonet, J.P.H. Sladen, L. Søby, L. Tanner, F. Tecker, J.C. Thomi, I. Wilson, G. Yvon - CERN

M. Bernard, G. Bienvenu, R. Chaput (LURE), J. Le Duff, T. Garvey, B. Mouton - LAL

Abstract

The design of CLIC is based on a two-beam scheme, where the short pulses of high power 30 GHz RF are extracted from a drive beam running parallel to the main beam. The 3rd generation CLIC Test Facility (CTF3) will demonstrate the generation of the drive beam with the appropriate time structure, the extraction of 30 GHz RF power from this beam, as well as acceleration of a probe beam with 30 GHz RF cavities. The project makes maximum use of existing equipment and infrastructure of the LPI complex, which became available after the closure of LEP.

In the first stage of the project, the "Preliminary Phase", the existing LIL linac and the EPA ring, both modified to suit the new requirements, are used to investigate the technique of frequency multiplication by means of interleaving bunches from subsequent trains.

This report describes the design of this phase.

CTF3 Design Report Preliminary Phase

1. INTRODUCTION

The CLIC design of an e^+/e^- collider aims at a centre-of-mass energy of 3 TeV and above, to be reached by acceleration with high gradients of 150 MV/m at 30 GHz with a pulse length of 140 ns. The RF power requirement is 240 MW per meter of linac length. Therefore a very efficient and reliable source of RF power is required. The scheme is based on a drive beam running parallel to the main beam, whose bunch structure carries a 30 GHz component. The RF power is extracted from the drive beam in Power Extraction and Transfer Structures and transferred to the main beam.

A novel scheme has been proposed, where the drive beam has a two-fold task: it converts a low RF frequency, where commercial power sources can be built, to 30 GHz and it compresses the RF energy, produced by klystrons in a long RF pulse, to a short pulse with a corresponding increase in peak power.

A long bunch train with low bunch repetition frequency is accelerated with low RF frequency. Subsequent packets of the bunch train are interleaved in isochronous rings thereby increasing the bunch repetition frequency and shortening the bunch train.

The main goals of CTF3 are to test this new RF power generation scheme and to produce 30 GHz RF power at the nominal peak power and pulse length, such that all 30 GHz components for CLIC can be tested at nominal parameters.

The facility will be built in the existing infrastructure of the LPI (LEP Pre Injector) complex and make maximum use of equipment becoming available after the end of LEP operation. The existing RF power plant from LIL (LEP Injector Linac) at 3 GHz will be used. The project is based in the PS Division with collaboration from many other Divisions at CERN, as well as from INFN Frascati, IN2P3/LAL at Orsay and SLAC.

Power efficiency is of utmost importance for CLIC, therefore the drive beam with high peak current is accelerated in fully-loaded cavities, such that almost all 3 GHz power is converted to beam energy. New accelerating structures are required with very strong damping of Higher Order Modes to keep the bunch trains stable. Since these new cavities will not be available before 2003, a proof of principle experiment of the bunch frequency multiplication scheme will be done, using the present accelerating structures from LIL. This first phase of CTF3 is known as "preliminary phase" [1] and is the subject of this report.

A first round of CTF3 experiments will start in autumn 2001 and will extend over the year 2002, with the goal to demonstrate the funnelling injection scheme and bunch train compression in an isochronous lattice. The main difference between these preliminary experiments and the nominal CTF3 is the limited beam current available from LIL, therefore 30 GHz RF power production and the study of collective effects will only be possible in later phases. In preparation for this, beam studies have already been done in 1999 and 2000 in order to verify the modelling of the optics characteristics of LIL and to demonstrate that the EPA (Electron Positron Accumulator) ring can be used as an isochronous ring [2].

2. GENERAL DESCRIPTION OF THE CTF3 PRELIMINARY PHASE

The general layout of the LPI complex before and after the modifications for the CTF3 preliminary stage is shown in Figure 2.1. Only electron operation is required, and the installation will become independent of the PS (Proton Synchrotron accelerator).

Present LPI

LIL

CTF2

EPA

LPI in 2001-2002

CTF3 Injector

CTF2

10 m

CTF3 Preliminary Phase
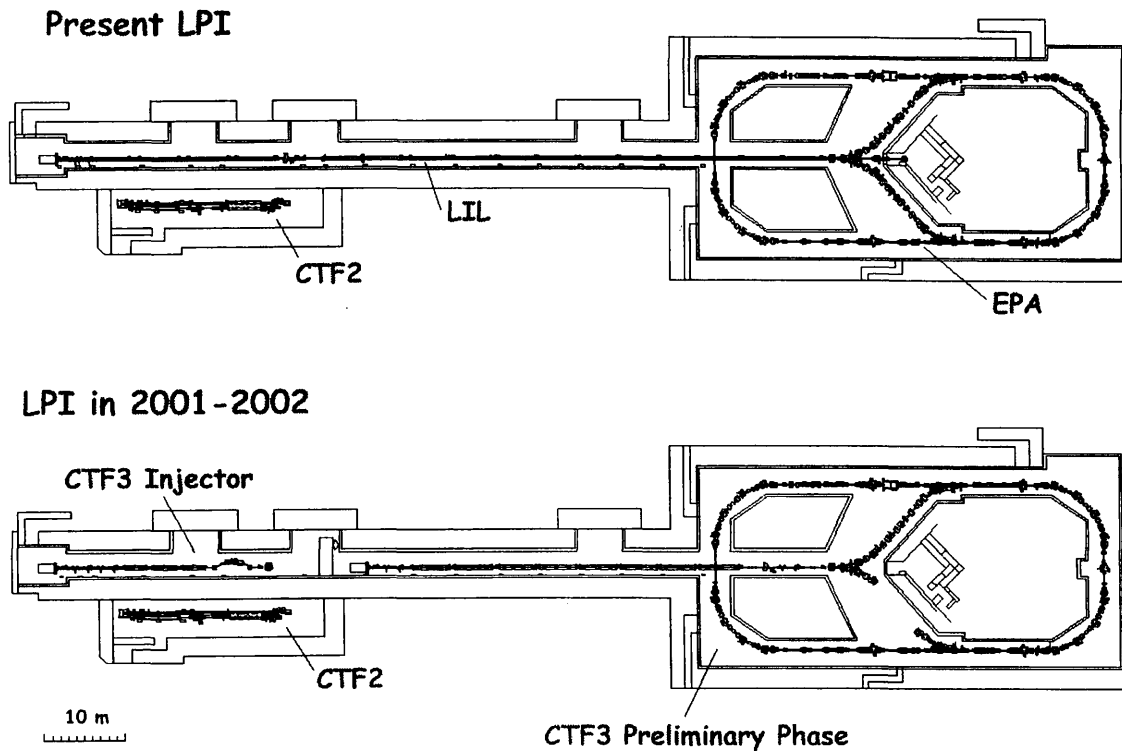
Figure 2.1: Conversion of present LEP Pre-Injector (LPI) to CTF3

3. GUN AND LINAC

Trains of up to seven pulses, each composed of several electron bunches, will be accelerated up to an energy of 350 MeV in the existing linac. For this, only eight of the presently installed sixteen travelling wave structures are required, powered in groups of four by two 40 MW klystrons. Since the maximum train length (2.5 μs) plus the cavities filling time (1.5 μs) is not much shorter than the RF pulse length from the klystrons (4.5 μs), the present RF pulse compression system LIPS (LIL Power Saver) will not be used.

The first part of LIL will be dismantled and the present front end with a new thermionic gun will be moved downstream to the location of the present LIL positron capture region. A new independent, shielded area will thus be created allowing the installation and commissioning of the new injector required for the later CTF3 phases, independent of the preliminary phase. Eight of the sixteen accelerating structures of LIL will be removed, as well as the extraction lines to the PS complex and the positron injection line between LIL and EPA ring. A more detailed layout is

shown in Figure 3.1. The beam parameters have been chosen in order to minimise the energy spread generated by beam-loading in the LIL structures, while still keeping the charge per bunch high enough to give a good resolution for the measurements of the beam time structure with a streak camera. The last two LIL accelerating structures will be replaced by a matching section to the injection line.
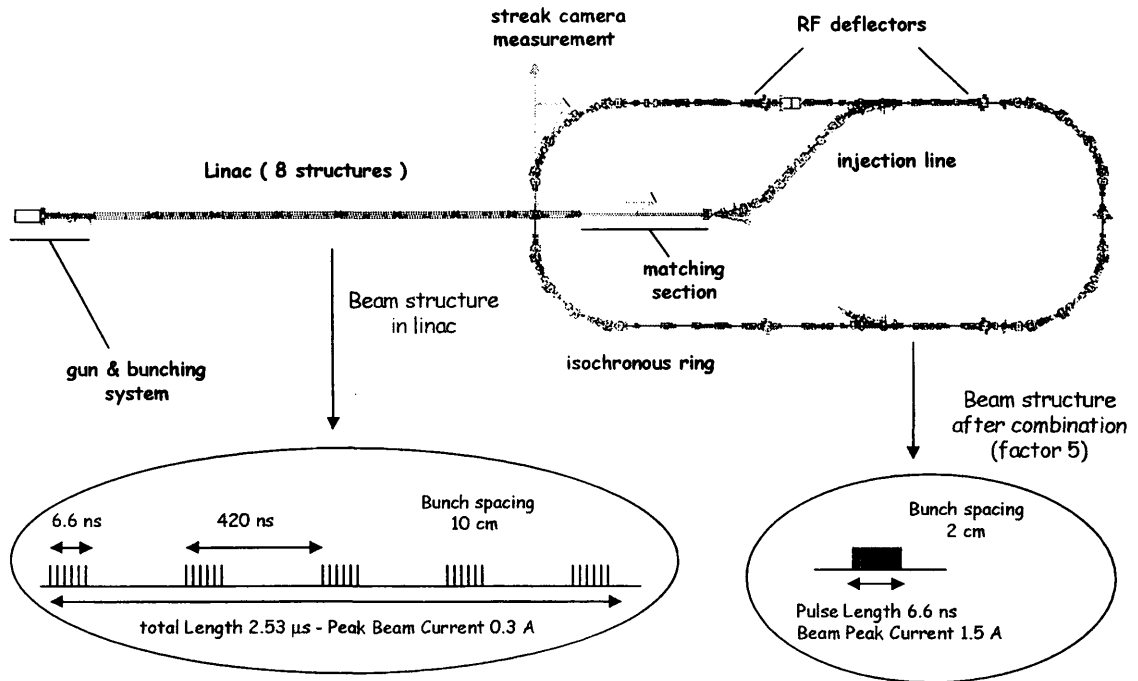
Figure 3.1: CTF3 layout with bunch structure

A new thermionic gun is required for the different time structure of the electron beam. It will provide a train of up to seven pulses. The nominal length of each pulse is 6.6 ns FWHM, and the pulses are spaced by 420 ns, corresponding to the EPA revolution time. This is shown in Figure 3.1. For the frequency multiplication test, one needs at most five pulses; two pulses out of the seven available can be dumped after acceleration in order to reduce the energy spread due to transient beam loading. The gun will be operated with a nominal peak current of 1 A. The present bunching system, powered independently by a 30 MW klystron, will provide a 3 GHz bunched beam at 4 MeV. Each pulse will then consist of 20 bunches, each of them having a charge of 0.1 nC and a length of about 10 ps FWHM.

3.1 Bunch combination

The EPA ring will be used for bunch combination. Injection into the ring will be done by means of RF deflectors. They create a time-dependent closed bump of the reference orbit, allowing the interleaving of three to five bunch trains. The circumference C of the EPA ring has to be such that the newly injected bunches can be placed between the already stored ones:

$$C = n\lambda_0 \pm \lambda_0 / N \quad (1)$$

where n is an integer number, λ_0 is the RF wavelength (10 cm), N is the combination factor (3, 4, or 5). The nominal value for N is four, but it can be chosen between three and five by changing the RF frequency. The principle is shown in Figure 3.2.
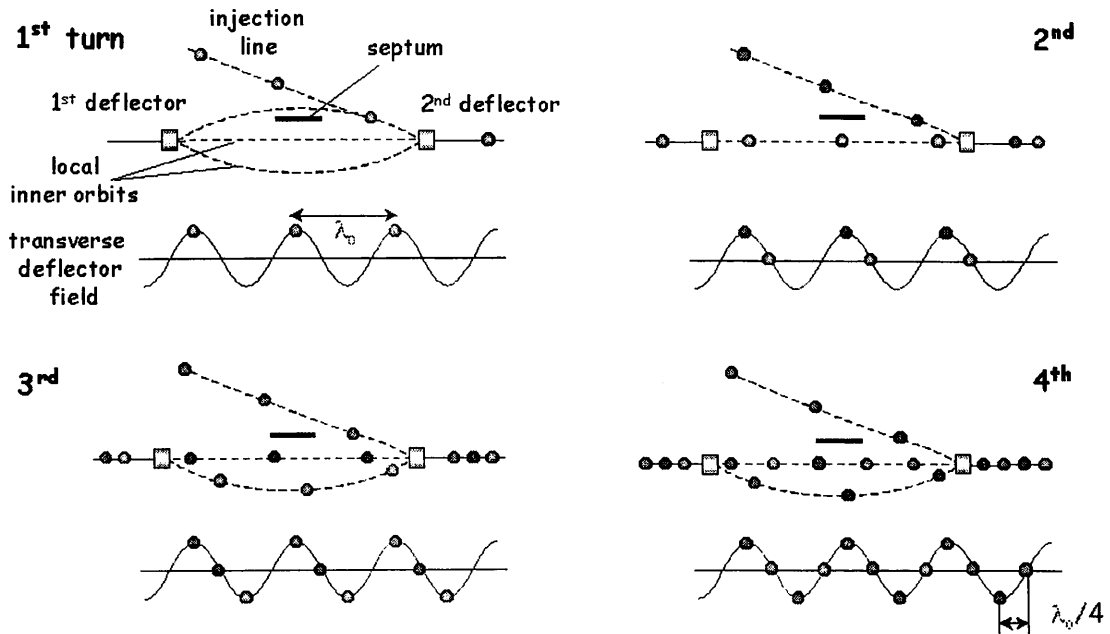
Figure 3.2: Bunch interleaving using RF deflectors

1) When the first train arrives, all of its bunches are deflected by the second deflector on to the equilibrium orbit.

2) After one turn, the bunches of the first train arrive in the deflectors at the zero-crossing of the RF field, and stay on the equilibrium orbit. The second train is injected into the ring.

3) After a second turn the first train bunches are kicked towards the inside of the ring, the second train bunches arrive at the zero-crossing, and the third train is injected.

4) On the third turn the first train bunches arrive again at the zero-crossing, the second train bunches are kicked into the inner orbit, the third train bunches are also at the zero crossing and the fourth train is injected. The four trains are now combined in one single train and the initial bunch spacing is reduced by a factor of four.

In order to maintain the short bunch length required, both the transfer line and the combiner ring must be isochronous.

In the transfer line, one quadrupole must be added to the present layout, and four of the existing quadrupoles must be moved. Independent power supplies will feed all eight quadrupoles in the transfer line. However, the overall geometry of the line is preserved, such that no major hardware modifications are needed.

The main modifications to EPA are a change in circumference of 17 mm and a rearrangement of several magnets (dipoles, quadrupoles, sextupoles). New families of quadrupoles and sextupoles are created.

3.2 Main parameters

The main parameters are given in Table 3.1.

Table 3.1: Main parameters

| Parameter	Value	Unit
Beam		
Repetition rate	50	Hz
Beam energy	350	MeV/c
Number of pulses/train	1-7	
Pulse duration	4-10	ns
Number bunches/pulse	12-30	
Bunch separation	0.33	ns
Bunch charge (flat top)	0.1-0.2	nC
Bunch length, FWHM	≤ 10	ps
Energy spread, total	≤ 2	%
Normalized emittance, rms	40	π mm mrad
Front-End		
Gun voltage	90	kV
Gun peak current	1-2	A
Pre-buncher voltage	47	kV
Buncher accelerating gradient	16	MV/m
Beam energy at front-end exit	4	MeV/c
Total RF power available	30	MW
RF – Linac		
Number of accelerating sections	8	
RF Frequency	2.99855	GHz
Number of Modulator-Klystrons	2	
Power per klystron	40	MW
RF pulse length	4	μs
Maximum β (including matching section)	200	m
Transfer line		
Momentum compaction	$\leq 10^{-2}$	m
Maximum β	200	m
Peak dispersion	1.2	m
Ring		
Combination factors	3-5	
Ring circumference	125.647	m
Momentum compaction (isochr, accumulation modes)	$\leq 5 \times 10^{-4}, 10^{-2}$	
Max path length deviation over $\Delta p/p = 2$ %	0.5	mm/turn
Maximum β	40	m
Peak dispersion	3 m	m
Tunes (horizontal, vertical)	4.73, 3.77	

4. MACHINE SYSTEMS

In the following section the major building blocks of the preliminary phase of CTF3 are described.

4.1 The front-end

The LIL front-end consists of a thermionic gun, a pre-buncher, a buncher, a matching section and beam diagnostics, as shown in Figure 4.1.
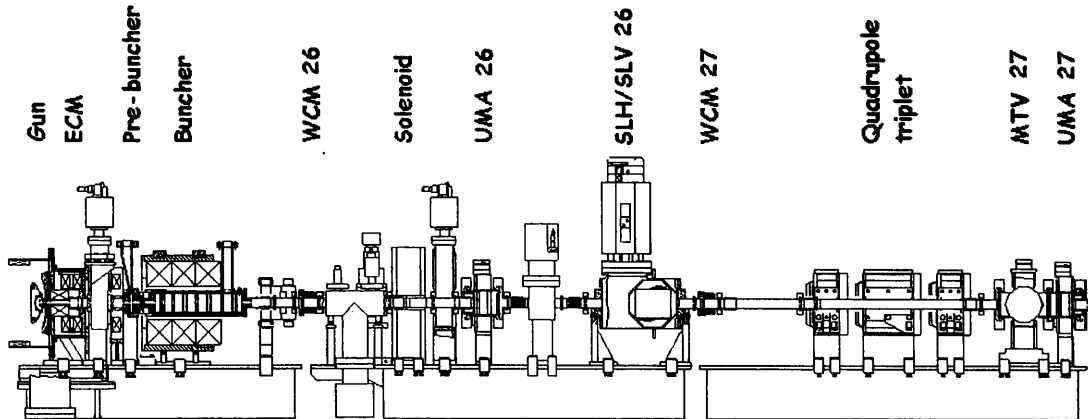
Figure 4.1: Layout of the new front-end

The required bunch structure after the injector is shown in Figure 3.1. The beam pulses consist of 20 bunches spaced by 10 cm. Up to seven such pulses follow each other at a distance of 420 ns. The repetition rate of these macro-pulses is 50 Hz. The main parameters of the front-end are given in Table 4.1.

Table 4.1: Main parameters of front-end.

RF frequency	2.99855	GHz
RF wavelength	0.099979	m
Nominal gun voltage	90	kV
Maximum gun voltage	100	kV
Nominal gun current	1	A
Maximum gun current	2	A
Repetition rate	50	Hz
Distance from pre-buncher to buncher	100	mm
Pre-buncher voltage	47	kV
Pre-buncher accelerating gradient	1.3	MV/m
Buncher accelerating gradient	16	MV/m
Available RF power	30	MW
Temperature of the bunching system	30	°C
Beam energy	4	MeV
Distance from buncher to ACS27	3.5	m
rms normalised beam emittance	40	π mm mrad
Bunch length(FWHM)	≤ 10	ps
Bunch charge	0.1	nC
Number of bunches / pulse	20	
Number of pulses	1 to 7	

4.1.1 The thermionic gun

Since the bunch structure cannot be produced with the existing equipment, a new thermionic triode gun is being developed under a collaboration agreement with LAL. The new design is based on a device already in use in the CLIO [3,4] machine. It will produce a train of seven pulses (2.56 μs in total) with a repetition rate of 50 Hz. Each pulse has a nominal length of 6.6 ns (FWHM), however, it can be varied in operation between 4 and 10 ns. The full train is 2.6 μs long. The main characteristics of the CLIO gun are given in Table 4.2.

Table 4.2: Parameters of the electron gun

Voltage	90	kV
Voltage (conditioning)	100	kV
Current	2	A
Train length	2.6	μs
Pulse length	4 to 10	ns
Rise time	< 2	ns
Time jitter (over 420 ns)	< ± 0.3	ns
Voltage stability	0.1	%
Normalised total emittance	< 15	π mm mrad
Repetition rate	50	Hz

4.1.2 The bunching system

The present bunching system of LIL will be used, consisting of a single-cell pre-buncher and a standing wave buncher, operating at a frequency of 2.99855 GHz. The pre-buncher is a 15 mm long pill-box cavity. The buncher is a 341 mm long 2π/3 standing wave structure. The parameters were optimised for a beam current of 3 A and a beam energy of 80 kV [5], however for the CTF3 parameters of 1 A and 90 kV no drastic changes are expected. The bunching efficiency will have to be tuned by adjusting the phase between pre-buncher and buncher as well as the amplitudes. The buncher will be powered by a 35 MW klystron, but only about 4 MW are necessary. The beam energy after the buncher is about 4 MeV.

4.1.3 The front-end matching section

In order to control the transverse beam dynamics, a solenoid and a quadrupole triplet with independent power supplies are installed after the bunching system. Since the new conditions are very similar to the previous ones, it is proposed to keep this configuration of the matching section in front of the linac.

4.1.4 Beam instrumentation

The beam instrumentation in the front-end is shown in Figure 4.1. A capacitive electrode (ECM25), located just downstream the anode, allows to measure the beam current before the bunching system. A Wall Current Monitor (WCM26) measures the beam current at the exit of the bunching system. The ratio of the currents measured in WCM26 and ECM25 gives the bunching efficiency. The horizontal and vertical slits SLH26 and SLV26 are used for machine development. The Beam Position Monitors UMA26 and UMA27 allow to check the transfer efficiency of the matching section and to align the beam in the first accelerating structure. They

are also used to calibrate the WCMs. Finally a TV Monitor with the scintillator screen (MTV27) allows to check the presence of the beam and to get an estimate of the transverse beam sizes.

4.2 The linac and the matching section

4.2.1 Linac

The first accelerating sections of LIL were removed. The new layout of the linac between the front-end and the matching section is shown in Figure 4.2
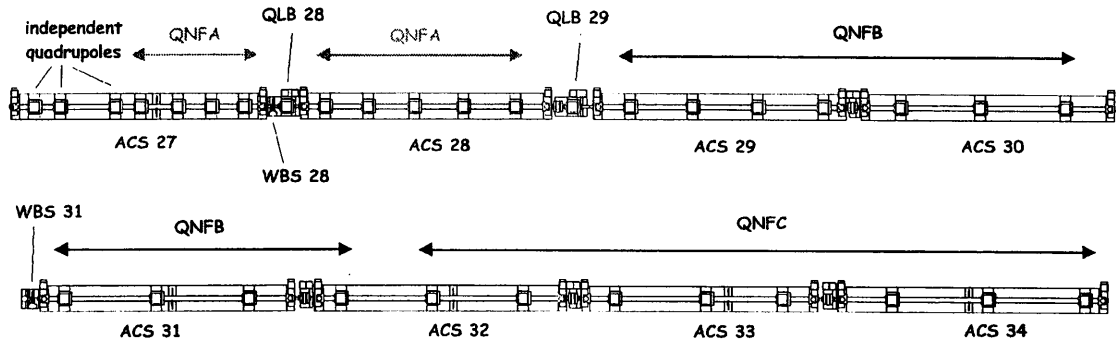
Figure 4.2: New layout of accelerating sections

The new linac optics was calculated using MAD [6] and Transport [7]. Since it is difficult to simulate the RF focusing in the first accelerating sections at the low energy of only ~ 4 MeV, the reference point was chosen just upstream of RF Accelerating Section ACS28. The Twiss parameters at the reference point can be inferred from measurements made on the present linac, assuming that the beam properties at the end of the new front-end remain the same as in the present situation. To achieve that, all quadrupoles on ACS27, as well as QLB28, should therefore be switched off. However, during the commissioning of the new linac, the values of the Twiss parameters just upstream of ACS28 may slightly differ from the ones used in this note. If necessary, the quadrupoles surrounding ACS27, as well as the triplet in the front-end, can be used to readjust the matching between the exit of the front-end and the entrance of ACS28. Based on measurements on the present linac, the following parameters at the reference point are assumed:

normalised rms emittance : 40 π mm mrad in both horizontal and vertical planes
energy before ACS28 : 47 MeV,
β_x = 8.7 m and α_x = +0.05
β_y = 11.9 m and α_x = -0.22

In order to reach an energy of 350 MeV in the EPA ring, each of the eight accelerating structures of LIL must provide an energy gain of 43 MeV.

The LIL accelerating structures are surrounded by quadrupoles. The effect of these quadrupoles is simulated in both Transport and MAD by the following procedure: acceleration up to the centre of the quadrupole, drift in the backward direction down to the entrance of the quadrupole, the quadrupole itself, drift in the backward direction down to the centre of the quadrupole, acceleration up to the exit of the quadrupole. A new treatment using a special element in MAD with analytically calculated transfer matrices has been recently implemented

and tested against measurements on the present linac [8] and gives similar results. It must be noted that while MAD takes into account the RF focusing in the accelerating structures, TRANSPORT does not. MAD seems to be more accurate. However, all the methods described here are in good agreement with the measurements made on the present linac, and the differences between their results were relatively small.

It is planned to keep all existing quadrupoles in their present position, except in the matching section starting just downstream of ACS34. The maximum values of the β functions along the linac are about 20 m, compared to a few hundred meters in the present LIL. It was verified that in the proposed optics the beam parameters are relatively insensitive to small changes of the initial conditions. The expected β functions are shown in Figure 4.3 and the positions and settings of the quadrupoles in the linac and the matching section are shown in Appendix 1.
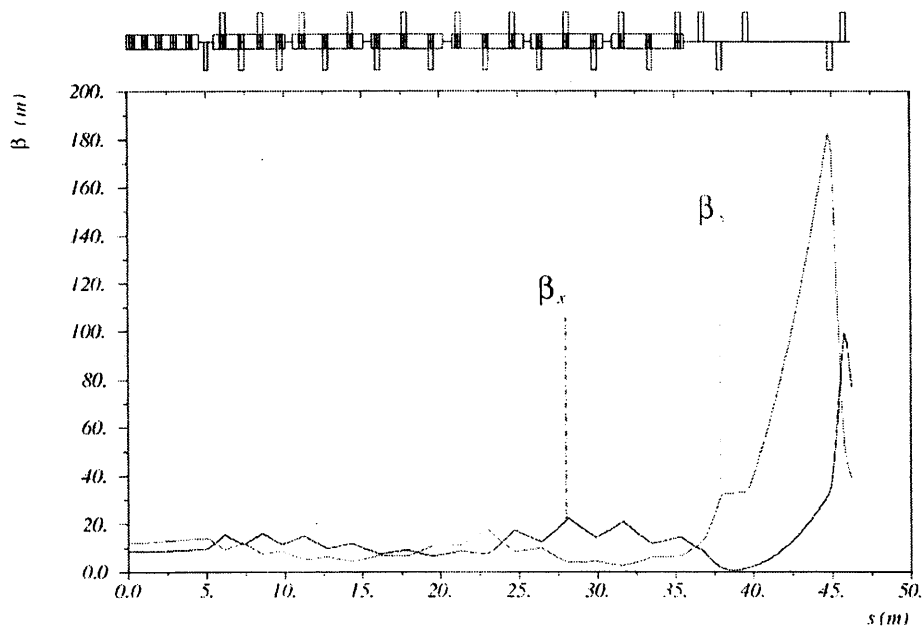
Figure 4.3: β-functions in LIL

4.2.2 Matching section

The matching section replacing the last two RF sections of the present linac is shown Figure 4.4.
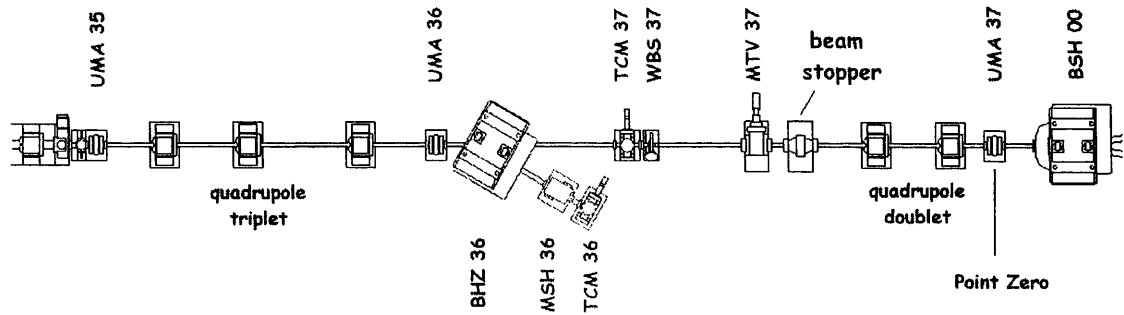
Figure 4.4: Matching section downstream of linac

The Twiss parameters at the end of the linac are imposed by the optics in the EPA ring and the transfer line. At the point referred to as zero, the Twiss parameters are:

$$\beta_x = 76.4 \text{ m}, \quad \alpha_x = + 29.4$$
$$\beta_y = 39.1 \text{ m}, \quad \alpha_y = +10.2$$

A good matching has been obtained by optimising the normalised gradient and the position of each of the five quadrupoles.

During the commissioning of the linac, the values obtained at the exit of ACS34 may be slightly different from what is assumed here. Consequently, some flexibility has been kept for the matching section, all quadrupoles being fed by independent power supplies. During the commissioning of the machine, accurate measurement of the beam parameters at the entrance of the matching section will be used to obtain a correct matching.

4.2.3 Beam instrumentation

Wherever possible the present beam instrumentation in the linac will be kept.

Beam position monitors (UMA) are placed between the accelerating structures, except at two locations, where Wire Beam Scanners (WBS) are or will be installed. Between ACS27 and ACS28, WBS28 is already installed. Another one (WBS31) will be placed between ACS30 and ACS31. These instruments will allow the measurement of the transverse beam characteristics (emittance and Twiss parameters) through quadrupole scans. In particular, using WBS28 and WBS31, it will be possible to check the beam parameters at the exit of the front-end and at the linac reference point upstream ACS28, respectively.

The matching section will be instrumented to provide a full characterisation of the beam before injection into EPA. The two UMAs at the beginning and end of the matching section (UMA35 and UMA37) will be kept at their present location, while the third (UMA36 currently located between ACS35 and ACS36) will be slightly displaced. A Wire Beam Scanner (WBS37) and a Transition-Cherenkov Monitor (TCM37) will be placed in the straight line. The WBS will allow the determination of the transverse beam parameters at the entrance of the matching section. In the TCM, a Transition Radiation screen or alternatively a Cherenkov screen can be put in the beam path. Together with an image frame grabbing system and digital treatment, the TCM can be used for the determination of the transverse beam parameters and will provide a way to cross-check the results of the WBS. The aim is eventually to use the TCM routinely for

emittance and Twiss parameters measurements. This will be done with an automated program derived from the one currently in use in CTF2, giving a much faster measurement than the quadrupole scan with a WBS. A camera (MTV37) will complete the instrumentation of the straight beam line.

A dipole magnet (BHZ36), will be installed in the matching section in order to deflect the beam into a spectrometer line. The line will be equipped with a SEM grid (MSH36) and a Transition-Cherenkov Monitor (TCM36). The nominal bending angle in BHZ36 will be 35°. Since the dispersion at the MSH location will be about 0.75 m, and the SEM grid wires are spaced by 2 mm, the energy resolution will be 0.3 %. With 20 wires, the acceptance on the MSH36 screen will be about 5 %. Assuming that β_x can be tuned down to 1 m in MSH36, with an rms normalised emittance of 40 π mm mrad, the rms beam size for a monochromatic beam should be around 0.2 mm and should thus not limit the spectrometer resolution.

An optical transport line will also be installed, in order to bring the light generated in TCM36 and TCM37 up to the streak camera laboratory. TCM37 could therefore be used for time-resolved measurements of the transverse beam parameters which can be useful, e.g. to study chromatic aberrations in the linac. The use of the streak camera with TCM36 will allow a time-resolved measurement of the beam energy spectrum. Using TCM36, where the dispersion will be about 1 m, we should be able to resolve pulse-to-pulse and bunch-to-bunch energy variations due to beam-loading.

4.3 CTF3 RF Power generation

The frequency of the CTF3 drive-beam accelerator will be 3 GHz instead of 937 MHz as in the CLIC scheme. This allows to use the 3 GHz klystrons, modulators, RF power compression units and the wave guide system from LIL for power production, with few modifications and with significantly less new equipment. The klystron-modulator (MDK) scheme is shown below in Figure 4.5.
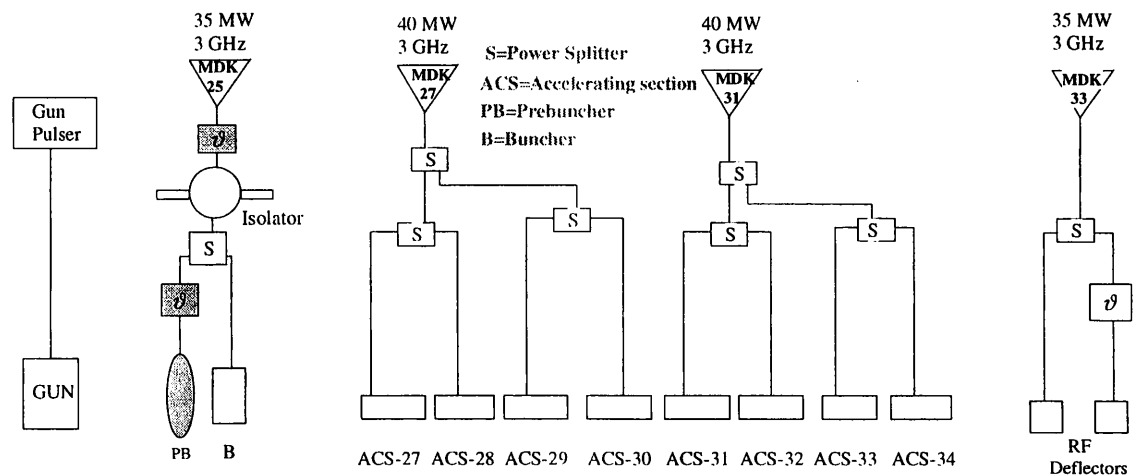
Figure 4.5: 3-GHz RF Power generation and distribution

Four klystron-modulators will be used in the preliminary phase of CTF3. The klystron-modulator MDK25 will provide RF power for the bunching cavities. This requires modifications to the

14

waveguide system, since the present LIL accelerating sections ACS 25 and 26 will be removed and the new injector installed upstream of section ACS27. The present klystron-modulator produces up to 35 MW peak output power and can be used as it is without modification. Since a rather long RF pulse (~ 4 μs) is needed, no RF pulse compression will be used. Therefore, the LIPS pulse compressors that are presently fitted to the output of all klystrons (not shown in Figure 4.5) for LIL operation, will be detuned.

The klystron-modulators MDK27 and 31 will use exactly the same RF waveguide networks and accelerating sections as they have for LIL, therefore reducing considerably the installation costs. In order to maximise the available peak RF power the internal configuration of these two klystron-modulators will be upgraded to 45 MW operation. This modification requires replacing the present 35 MW klystrons and their high voltage tank assemblies with complete 45 MW klystron assemblies from the CTF2 test facility. Lower impedance pulse forming networks (PFN's) must also be installed in order to efficiently match this higher power klystron to the modulator.

The fourth klystron-modulator (MDK33) is a new RF power source that was completed in 2000 for CTF3 operation. It has been built as a 35 MW system and uses parallel connected, compact, high-voltage switched mode power units for recharging its PFN. This reduces considerably the space required in the LIL gallery compared to the existing klystron-modulators, and is also very cost effective. The MDK33 system will be connected to the two RF deflectors to be installed in EPA (x5 combiner ring). A new waveguide system, ~70 m long with SF_6, from MDK33 to these deflectors is needed. This new system has been designed for operation at a nominal 50 Hz rate for CTF3. Table 4.3 below gives the important CTF3 klystron-modulator parameters.

Table 4.3: Parameters of the 3-GHz RF system

Parameter	Value	Units
Centre frequency	2998.55	MHz
Repetition frequency (nominal)	50	Hz
35 MW Klystron		
35 MW klystron peak beam voltage	270	kV
klystron peak beam current	286	A
micro-perveance	1.9 to 2.05	$A/V^{-1.5}$
PFN impedance	~5.5	Ω
PFN charging voltage	40	KV
Pulse transformer ratio	1:13	n
45 MW Klystron		
45 MW klystron peak beam voltage	304	KV
klystron peak beam current	334	A
micro-perveance	1.9 to 2.1	$A/V^{-1.5}$
PFN impedance	~4.0	Ω
PFN charging voltage	40	kV
Pulse transformer ratio	1:14.8	n

4.4 Reference Line and Klystron Synchronisation

For the preliminary phase of CTF3, the following klystrons of LIL will be used for driving the ACS (accelerating sections) built for LIL, which will be powered by a rectangular RF-pulse of 4 µs duration and 50 Hz repetition rate:

MDK 25	for Pre-buncher and Buncher
MDK 27	for ACS 27-28-29-30
MDK 31	for ACS 31-32-33-34
MDK 33	for two RF-deflectors in EPA

All four klystrons will be driven by the reference line of LIL, which delivers the correct frequency, phase and power to each klystron. The reference line running parallel to the accelerator beam line will be used for the preliminary test phase of CTF3 in the same configuration as for LIL. The reference line is driven by the klystron source TH2452 in the gallery, providing RF power of 17 kW. About 2 kW is tapped off from the reference line by power couplers for driving each klystron. In order to reduce the RF power and to prolong the lifetime of the reference klystron, the power couplers for the unused MDK03 and MDK13 will be removed from the reference line, resulting in a power saving of 25% for the reference klystron. For RF conditioning of the accelerator CTF3, the pulse repetition rate of the reference klystron can be set to 100 Hz.

For the preliminary phase of CTF3, the LIPS pulse compression system is not required. The LIPS cavities installed at MDK25, MDK27 and MDK31 will be detuned. The three klystrons MDK25, MDK27 and MDK31 are equipped with the electronics for phase control (called box A), for pulse length control (box B), and with equipment for measuring the amplitude envelopes (box C) of the RF-pulses. The RF-power at the input of the pre-buncher and buncher will be monitored by the existing RF-cables of sections ACS 25 and ACS26. The phase shifter and the power attenuator will be removed from MDK13 and installed on MDK25. The electronics chassis for the remote control of the WG-power-attenuator and the WG-phase-shifter of the pre-buncher will be transferred to rack RA62 and connected to the controls system.

Only the new klystron MDK33 must be equipped with a new box A, which will be connected to the reference line using the existing coupler of MDK35. Box A for MDK33 will be taken from the beam position measurement of CTF2, where a digital phase shifter 3GHz will be installed, replacing box A. The box B for MDK33 comes from MDK03. The power inputs PSI/R of the RF-deflectors will be monitored by two bi-directional WG-couplers coming from ACS25 and ACS26, and 4 RF-cables must be installed from the RF-deflectors to MDK33, box A and box C. The rack RA125 has been reserved to install the electronics chassis of the boxes A, B, C for MDK33.

4.5 The transfer line HIE between the linac and the ring

The design of the transfer line between the linac and the EPA ring has to meet several requirements:

* It has to be isochronous in order to avoid direct bunch lengthening.

* The transverse Twiss functions have to be matched at both ends of the line, as well as the horizontal and vertical dispersion functions and their derivatives.

* Small β-functions, well below the present values of a few kilometres, are required in order to keep chromatic effects small.

4.5.1 Requirements

The requirements on the new injection line are more stringent than for the existing one, in particular transverse and dispersion matching must be very precise due to the aperture restriction of the RF deflectors in the ring and because of the achromaticity condition.

To first order, the evolution of the bunch length through the transfer line is controlled by the coefficients of the linear 6 x 6 transfer matrix R. When neglecting vertical dispersion, which is indeed much smaller than the horizontal dispersion in the transfer line, the path length difference of a given particle with a relative momentum difference $\Delta p/p$ with respect to the reference particle is given by:

$$c\Delta t = R_{51}x + R_{52}x' + R_{56}\frac{\Delta p}{p} \tag{2}$$

Here (x, x') refers to the usual horizontal phase space at the entrance of the line and, for a reference path L along the line, the matrix coefficients are defined by:

$$R_{51} = \int_L \frac{C}{\rho}, \quad R_{52} = \int_L \frac{S}{\rho}, \quad R_{56} = \int_L \frac{D}{\rho} \tag{3}$$

where ρ is the bending radius, C and S are the cosine-like and sine-like principal solutions of Hill's equation of motion, and D is the horizontal dispersion.

For the rms bunch length σ_l, the following equation can be obtained:

$$\sigma_{lf}^2 = \sigma_{li}^2 + (R_{56}\sigma_E)^2 + \varepsilon_{xi}(R_{51}^2\beta_{xi} - 2R_{51}R_{52}\alpha_{xi} + R_{52}^2\gamma_{xi}) \tag{4}$$

In this equation σ_E is the rms energy spread. The subscript i refers to the entrance of the transfer line, while the subscript f can refer to any point downstream.

The matching of the horizontal dispersion and its first derivative at both ends of the transfer line requires a first order achromat: $D_{xi} = D'_{xi} = 0$ are the values of the dispersion and its derivative at the entrance of the line (end of the linac) while $D_{xf} = D'_{xf} = 0$ are their values at the end of the line (injection point in the EPA ring). For such boundary conditions, it can be shown that R_{51} and R_{52} vanish:

$$D_{xi} = D'_{xi} = 0$$
$$D_{xf} = D'_{xf} = 0$$
$$\Longrightarrow R_{51} = R_{52} = 0$$

From equations (2) and (4), the last condition to fulfil is the first-order isochronicity, i.e. $R_{56} \cong 0$. This requires the modification of the horizontal dispersion function along the transfer line, in order to force the ratio D/ρ to change sign, so that the third integral of equation (3) vanishes over the total path length. The new design of the transfer line was mainly driven by this condition, and by the fact that the new layout should only generate minor modifications to the existing hardware.

4.5.2 Layout

In the new configuration, the dipole magnets are neither moved nor changed compared to the present situation of the transfer line. However, two new focusing quadrupoles are needed in

order to control the value of R_{56}: one upstream of the dipole BHZ10, near the beginning of the line, and the other one downstream of the dipole BHZ30, just before the first injection septum. The positions and the normalised gradients of the existing quadrupoles are modified. In the central straight part of the line, one existing quadrupole is removed and four out of five quadrupoles must be moved. Independent power supplies will feed all 8 quadrupoles in the transfer line.

The modifications of the layout and of the optics for the new transfer line are summarised in Figure 4.6 and Appendix 2. In this solution, all quadrupoles are used in a global way to cope with all constraints: the small R_{56} factor, the horizontal and vertical dispersion matching and the transverse Twiss parameters behaviour. A different optics was studied, with no dispersion in the central straight part of the transfer line. This had the advantage of partially decoupling the transverse and longitudinal matching, but it was abandoned because it is not feasible with the existing hardware.
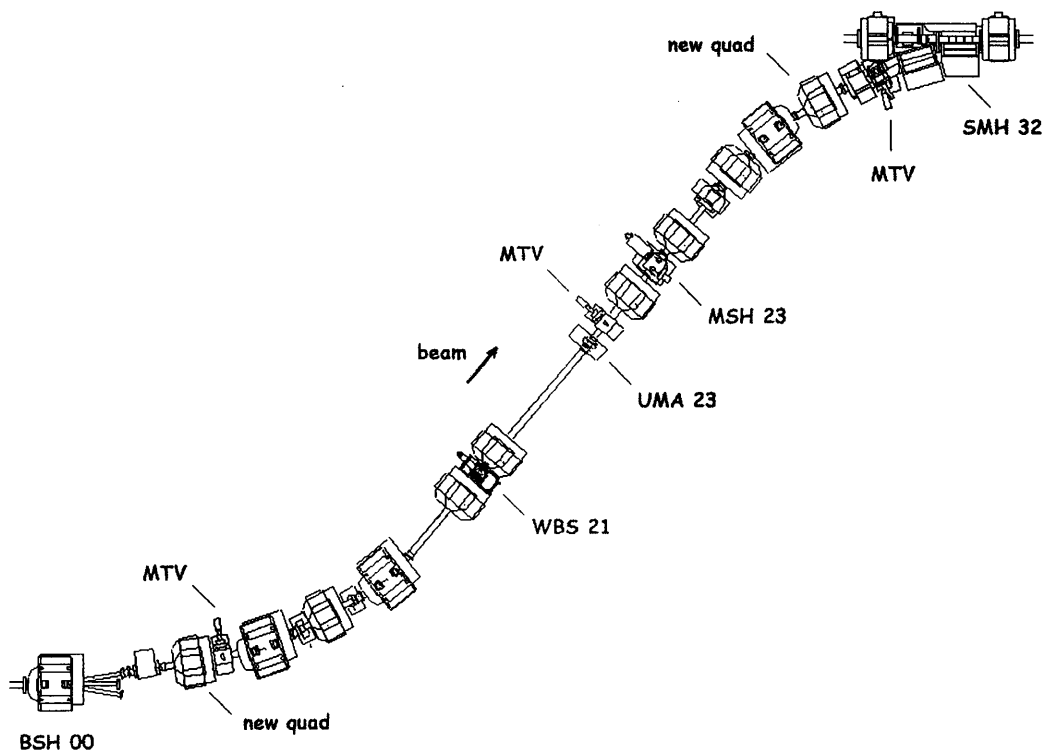
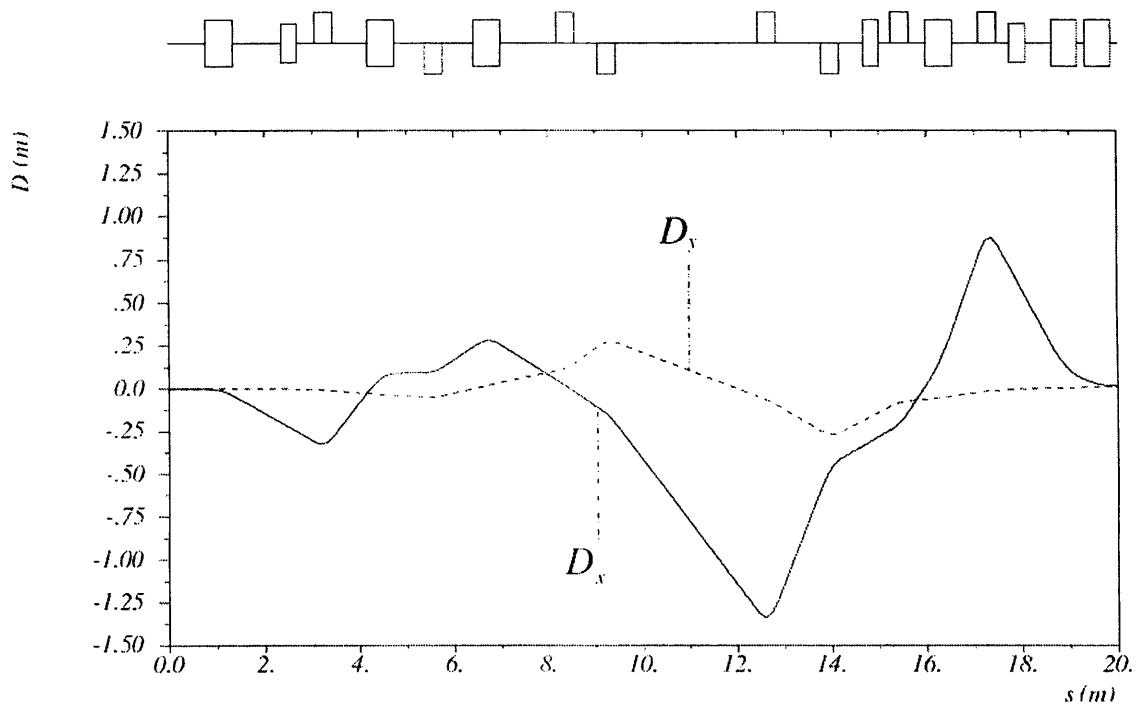**Figure 4.6: Transfer line between the linac and the ring**

The Twiss functions of the new lattice are shown in Figure 4.7 while the dispersion functions are shown in Figure 4.8. The vertical dispersion differs from zero because of the two vertical bending magnets used to match the LIL and EPA heights.
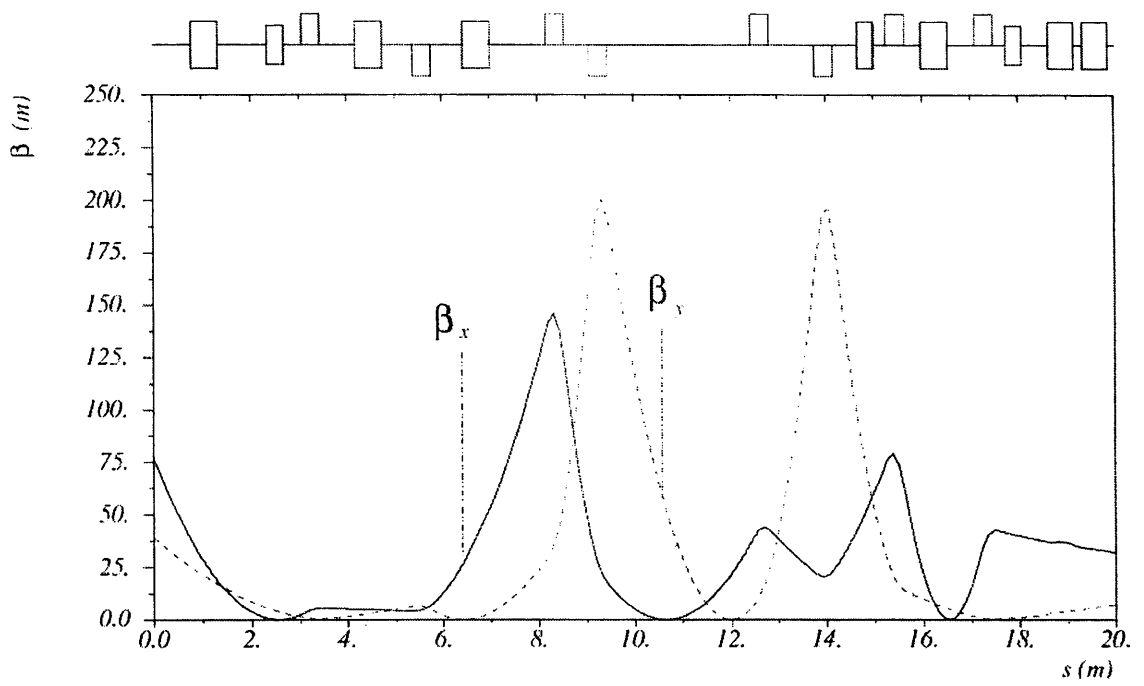
**Figure 4.7: Twiss Functions of transfer line**

Figure 4.8: Dispersion functions of transfer line

19

This configuration allows a quasi-isochronous operation with $|R_{56}| \leq 10^{-2}$ m, compared to $R_{56} \cong - 1$ m before the transformation. Shown in Figure 4.9 is the variation of the path length in the transfer line with the relative momentum deviation, for a zero emittance beam (left hand side) and for a beam with the nominal emittance (right hand side).
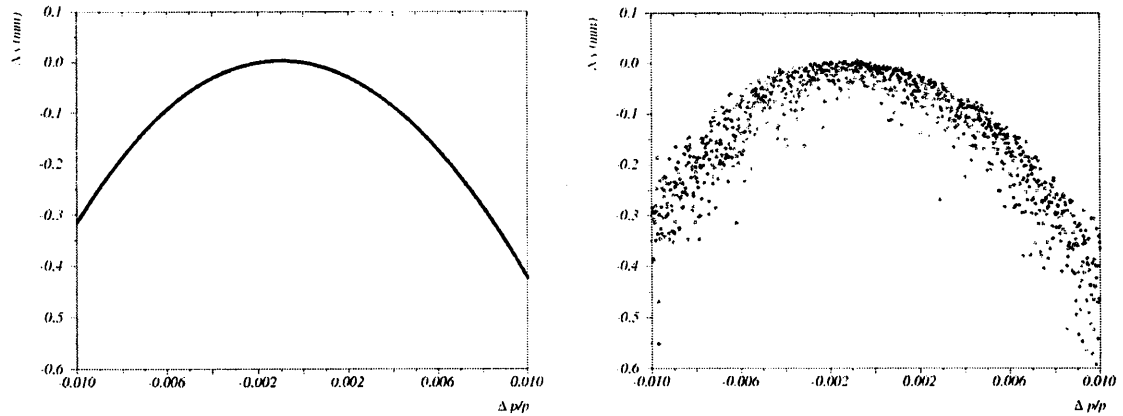
Figure 4.9: Path length difference for particles with different momentum deviations

This figure shows that the first order isochronocity is very small and that the dominant effect is the second order isochronicity. Such an effect is still acceptable and no corrections with sextupoles are needed. The effect of the emittance is shown on the right-hand side of the figure: it is visible but it remains small. As a consequence, no significant bunch lengthening is observed between the entrance and the exit of the line. However, along the transfer line, the bunch length varies according to equation (4): it grows in the first bends, reaches a maximum in the central straight part of the line and then decreases in the last bends, following the value of R_{56}. Figure 4.10 shows the evolution of the bunch length as a function of the curvilinear abscissa in the transfer line.
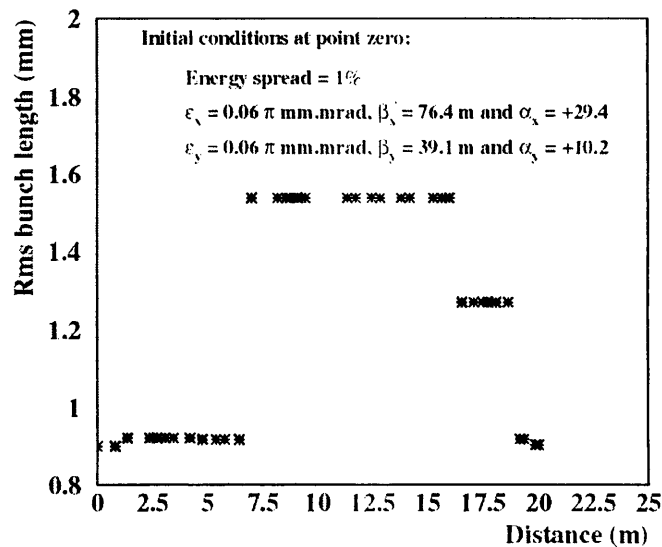
Figure 4.10: Bunch length variation in transfer line.
(ε_x and ε_y are the geometrical emittances)

20

The beam properties in the transverse plane at the beginning of the transfer line are imposed by the values of the Twiss parameters needed to match the transfer line to the EPA ring. At the injection point (15 cm downstream the exit of the septum SMH32), they are:

$$\beta_x = 31.2 \text{ m}, \quad \alpha_x = +2.2$$
$$\beta_y = 7.0 \text{ m}, \quad \alpha_y = -1.6$$

Therefore, knowing the transfer matrix of the new transfer line, the Twiss parameters needed at the end of the linac (point zero) can be derived. Their values are the ones used in section 4.2.2 . They are reported in Figure 4.10.

4.5.3 Beam diagnostics in the transfer line

The beam diagnostics elements of the transfer line are shown in Figure 4.6.

Three television cameras (MTV) are distributed along the line: the first one is located upstream of BHZ10 in the first bending region, the second one is in the straight section upstream of QFW23, and the last one is downstream of BVT30, before the injection septa. These screens will help to follow the beam through the injection line.

A WBS is located between the quadrupoles QFW21 and QDW22 in the straight section. In the proposed optics, this position corresponds to a zero-crossing region of the dispersion function with high values of the β functions in the vertical and horizontal planes. This allows quadrupole scans to characterise the transverse behaviour of the beam and to make comparisons with the design optics.

A SEM grid is also located downstream in the central straight part of the line, between the quadrupoles QFW23 and QDW24, in a region with high dispersion, in order to check the value of the dispersion and to measure the mean energy and the energy spread at this point.

4.6 The EPA ring with isochronous optics

4.6.1 Isochronous optics in the old EPA ring

The momentum compaction factor of the old EPA optics ($\alpha = 0.034$), combined with a momentum spread of $\pm 1\%$ does not allow the injected bunches to remain short enough after five turns for the purposes of the CTF3 tests. The path length differences between the particles with extreme momenta in the bunches exceeded 80 mm per turn, which was too large by more than two orders of magnitude to preserve FWHM bunch lengths in the 10 ps range. In a first test in 1999, using existing magnets and cabling, the EPA optics was modified to yield $\alpha = 0$ [9]. Using the chromaticity sextupoles, the path length could be controlled to within 0.035 mm per turn across the momentum range of the bunches, while keeping the horizontal and vertical chromaticities close to zero. Unfortunately, the dispersion could not be cancelled in the injection region with the existing quadrupole layout and powering. This resulted in a dispersion mismatch between the injection line and the ring, and the injection efficiency was smaller than with the old nominal optics. Equally, the single turn path lengths were modulated by this mismatch, thus perturbing the evolution of the bunch length over the first few turns.

4.6.2 Isochronous optics with the modified EPA ring (Recombination mode)

In the CTF3 preliminary phase, the constraint of lepton production for LEP disappears and it will become possible to move or reconfigure the quadrupole families. The proposed optics will limit the transverse beam sizes in the small aperture RF dipoles (see Figure 4.11). On top of small β_x and β_y values, this requires $D_x = 0$ in the injection straight sections.

With the new optics, the symmetry in each of the four arcs with respect to their centre is abandoned. All six quadrupoles in each arc will be powered individually, increasing the number of arc quadrupole families from three to six. The symmetry of the ring with respect to the centre of each of the four straight sections between the arcs is preserved. By choosing appropriate integer tune values, the required gradients could be kept at a moderate level and the new isochronous optics can be achieved with the present magnets up to a beam energy of 400 MeV. The strengths of the quadrupoles in the long straight sections are unchanged, in order to keep the beam sizes and trajectories close to those of the nominal EPA optics. In order to better match the arc optics to the straight section optics, one quadrupole (QFWb) in each arc must be displaced by 1.85 m towards the long straight section. The new layout of one EPA arc is shown in Figure 4.12, Appendix 3 gives the normalized gradients of the quadrupoles.
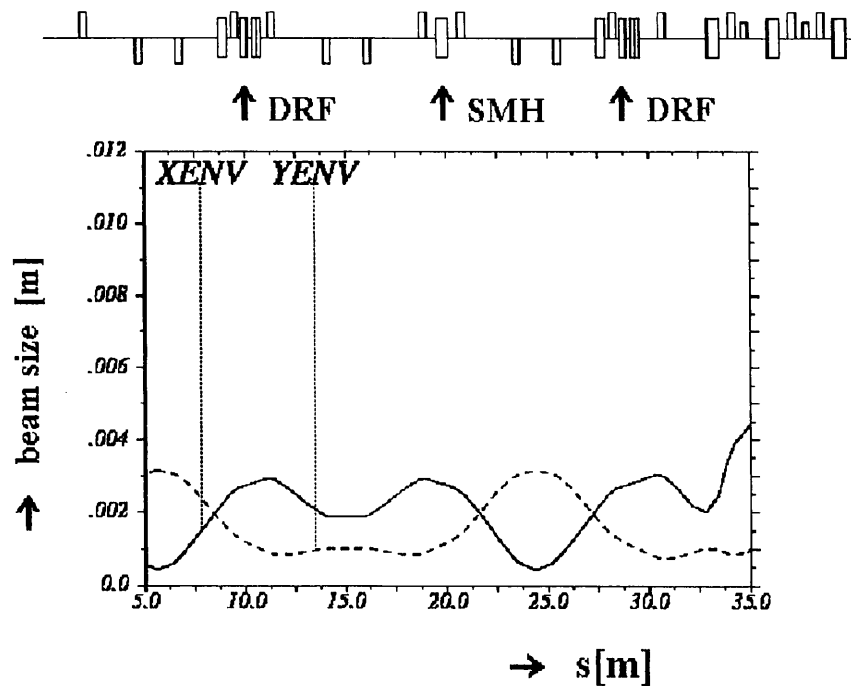

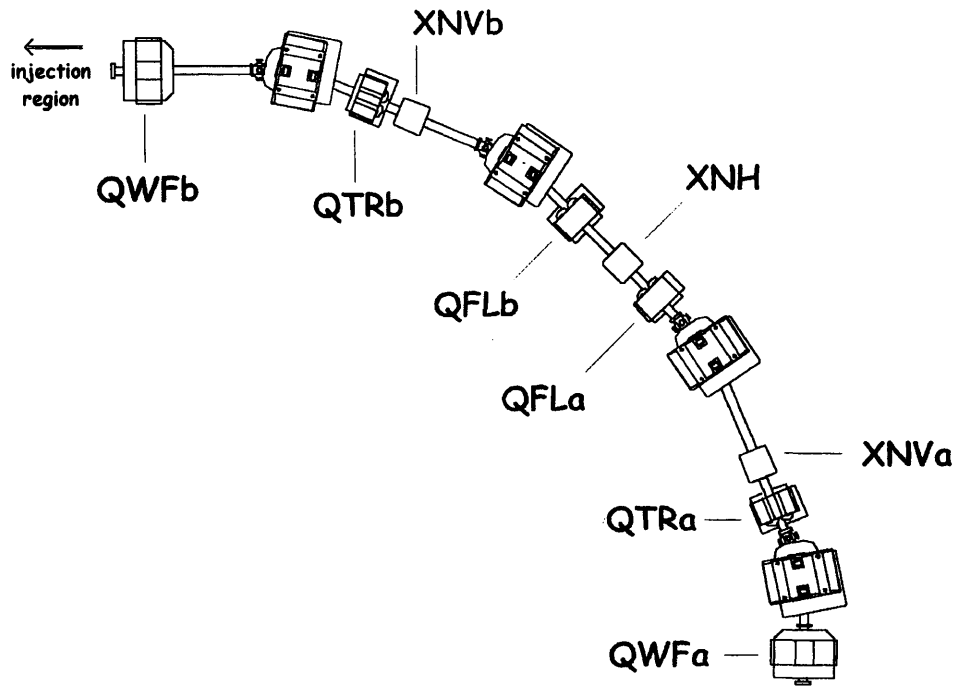**Figure 4.11: Beam size in the region of the RF deflectors**

Figure 4.12: Modified arc geometry in EPA

Figure 4.13 shows the horizontal and the vertical β-functions, as well as the dispersion function, in one arc of the new isochronous EPA ring.
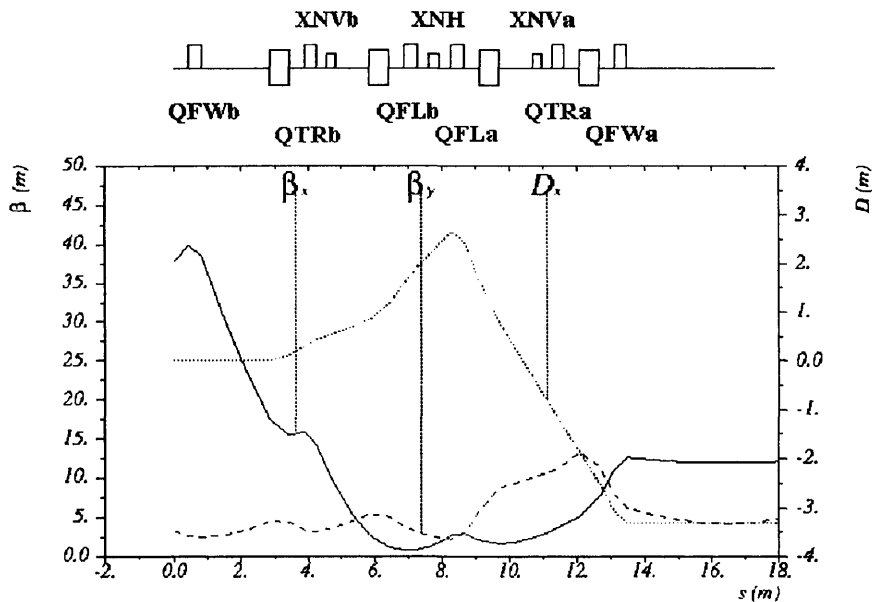

Figure 4.13: β-functions and dispersion in modified EPA ring

4.6.3 Non-isochronous optics with the modified EPA ring (Accumulation mode)

In addition to the isochronous optics ($\alpha = 0$), another optics, with $\alpha = 0.034$, has been designed to be used during the commissioning of the new EPA ring. This optics will allow the RF system to keep a stored beam circulating for beam optics optimisation and diagnostics purposes. In this case, the values of the normalised gradients of all quadrupoles are those given in Appendix 4.

4.6.4 Change of the EPA circumference

The nominal RF frequency is 2.99855 GHz, which corresponds to a wavelength $\lambda_0 = 0.099979$ m. The circumference of the present EPA ring (nominally $40\,\pi$ m, confirmed by recent measurements [10] is thus equal to 1256.9 λ_0. Bunch train recombination over three, four or five turns in EPA requires circumferences of 1256.666 λ_0, 1256.750 λ_0 or 1256.800 λ_0 respectively. To keep these three options open with the same ring layout, an average circumference value of 1256.73 nominal wavelengths has been chosen. The required reduction of the EPA circumference is thus equal to 0.17 λ_0, i.e. 17 mm. In order to switch between three, four or five turn recombination, the RF frequency will be slightly detuned.

4.6.5 Performance

The isochronous optics for EPA provides $D_x = 0$ in the two injection long straight sections (see Figure 4.13), but a non-zero horizontal dispersion in the two other straight sections. The transfer matrices between injection elements are the same as in the nominal machine. The beam sizes in the RF dipoles remain sufficiently small compared to their physical aperture (the smallest diameter is 21 mm).

The natural chromaticities of the new isochronous optics are comparable to those of the nominal EPA optics. The off-momentum path lengths can be controlled using the chromaticity sextupoles (now organised in three families instead of two) to within 0.5 mm per turn across the momentum range of the bunches, while keeping the chromaticities small. (See Figure 4.14 and Figure 4.15). This was already done in an experiment in EPA in 1999 [9]. Tracking over 1000 turns shows horizontal and vertical dynamic apertures around 15 σ across the momentum range of the incoming beam.
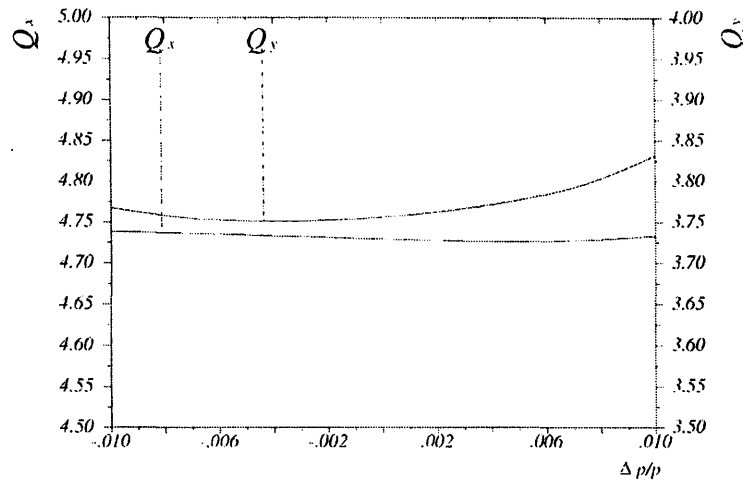
Figure 4.14: Horizontal and vertical tunes versus relative momentum deviation
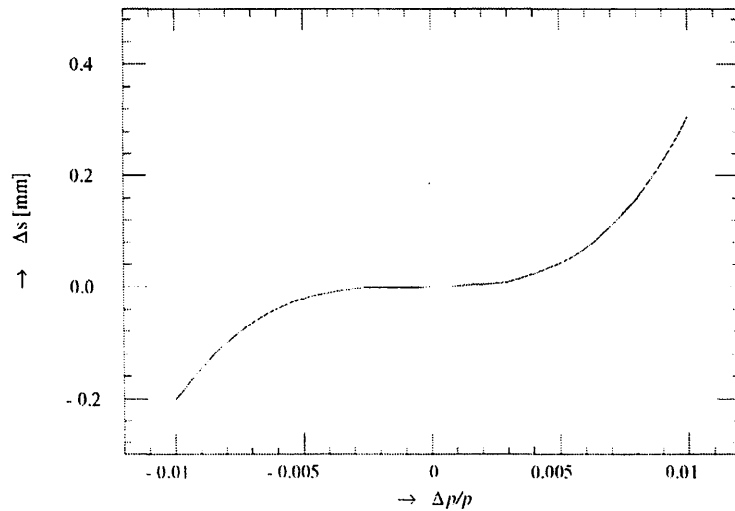
Figure 4.15: Variation of one-turn orbit length with relative momentum deviation

4.6.6 Beam diagnostics in the EPA ring

The existing instrumentation in EPA will be used in the preliminary phase of CTF3 with several modifications. The quadrupole (QFI82) after the injection septum is too close to the Wire Beam Scanner WBS82, and can thus not be used for measurements on the incoming beam. WBS82 will be moved further downstream so that quadrupole scans can be done at injection to check the transverse matching of the injected beam to the EPA ring optics.

Furthermore, the existing optical lines used to transport the synchrotron radiation signal to the streak camera will be modified. Since positrons will no longer circulate in the EPA ring, the optical lines can be simplified: some semi-transparent elements can be dismantled, increasing the amount of light available. Three light ports, located in the bending magnets BHZ52, BHZ56 and BHZ58, with values of the dispersion ranging from 0 to about 3 m, will be used. A moving mirror will be installed. Therefore part of these optical lines can be in common with the optical lines used for TCM36 and TCM37, which are located in the matching section. It must be noted

that the synchrotron light measurement with the streak camera is the main diagnostic tool available to observe the beam time structure in detail. As shown in previous tests in EPA [2], the precise tuning of the ring optics to isochronicity can be obtained rather easily by using the streak camera to observe the bunch length and distance over several turns. The streak camera measurement will eventually be the tool to demonstrate the bunch combination process. The nineteen Beam Position Monitors in EPA are used without hardware modifications. More details on their use can be found in section 4.10.

4.7 Injection using RF deflectors

In order to achieve bunch frequency multiplication, the bunch trains are injected in the isochronous EPA using two RF deflectors which are placed in the ring with a betatron phase advance of π between them, so that they produce a time-dependent closed bump (see Figure 3.2 for details).

Present LPI Injection Region

CTF3 Preliminary Phase Injection Region
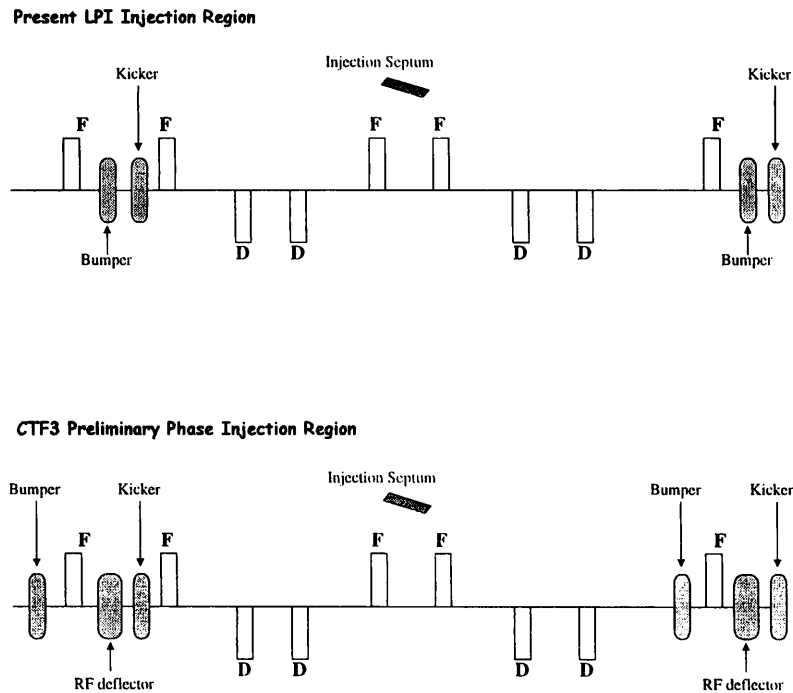
Figure 4.16: Injection region

The present injection scheme is shown in Figure 4.16. It uses a pair of static dipoles (bumpers) to bring the orbit close to the septum and two fast kickers for the fast injection. The bumpers, as well as the kickers, have a phase advance of π between them. In 2002, two RF deflectors will be installed at the locations of the bumpers. The kickers will not be moved, while the bumpers will be slightly displaced. The RF deflectors, whose positions are also shown in Figure 4.16, will be used instead of the kickers for the bunch combination tests.

4.7.1 The RF deflectors

For the CTF3 preliminary phase, the RF deflectors are short, travelling wave, iris-loaded structures for which the fundamental mode is a deflecting mode, with a phase advance of $\pi/2$ per cell and a negative group velocity [11]. Each deflector has an overall length of 27 cm, with six regular cells (and the two couplers) and an iris diameter of 2.3 cm (2.1 cm in the coupler cells). In this type of cavity, the deflecting force is uniform in strength and direction over the aperture [12]. The voltage attenuation along the structure is characterised by the constant α and the deflection angle is given by:

$$\phi = \frac{\sqrt{ZP}}{E}\left(\frac{1-e^{-\alpha L}}{\alpha}\right)$$ (5)

where P is the input power, L is the total active length, E is the electron beam energy, and Z is the series impedance defined as:

$$Z = \frac{R}{Q}\frac{2\pi}{\lambda_0}\frac{1}{\beta_g}$$ (6)

where R is the shunt impedance, λ_0 is the RF wavelength, Q is the quality factor, and β_g is the normalised group velocity.

Table 4.4: Main Parameters of the RF Deflectors

Parameter	Symbol	Value	Unit
Frequency	v	2.998	GHz
Number of cells	N_c	6+2	
Dephasing / cell		$\pi/2$	
Opening	$2a$	2.3	cm
Diameter	$2b$	11.9	cm
Cell length	d	2.5	cm
Active length	L	20	cm
Overall length	L_d	27	cm
Normalised group velocity	β_g	−0.0189	
Quality-factor	Q	1.281×10^4	
Shunt impedance	R	3.389×10^7	Ω/m
Series impedance	Z	8.797×10^6	Ω/m
Voltage attenuation	α	0.13	m^{-1}
Input power	P	7	MW
Deflection angle	ϕ	4.5	mrad

When using the parameters given in Table 4.4 a reference injection angle of 4.5 mrad is found for a 7 MW input power (the two couplers are considered as two active cells for the transverse deflection). The main drawback of the existing RF deflectors is their limited aperture. Therefore, new deflectors with a larger aperture are being built by INFN Frascati for later phases of CTF3, but could possibly become available already in 2002 [13].

4.7.2 Injection scheme

The angle required for injection is given by both the geometry of the injection region and the optics. If μ_x is the horizontal phase advance between the deflector and the septum, and β_s and β_d are the values of the horizontal β function at the septum and the deflector locations, then the angular kick is:

$$\theta = \frac{x}{\sqrt{\beta_s \beta_d} \, \sin \mu_x} \tag{7}$$

where x is the distance between the centre of the injected beam and the centre of the machine aperture at the location of the septum. Given the geometry of the vacuum chamber in this region, and taking into account the radius of the chamber (around 47 mm) and the septum thickness (around 10 mm), the distance x must be larger than 57 mm. Using equation (7), the required deflection angle is of the order of 4-5 mrad.

The maximum angular kick is needed for the injected beam, so that the centre of the injected bunch is on the crest of the cosine deflecting field in the RF deflector. For a frequency multiplication factor of five, the centres of the four circulating bunches are located on the curve of the deflecting field with phases of $2\pi/5$, $4\pi/5$, $6\pi/5$, $8\pi/5$ from the crest. Figure 4.17 shows the variation of the kick with the location of the bunches on the cosine curve. The extension is indicated for $\pm 2\sigma$ of a Gaussian distribution with a length of 10 ps FWHM.
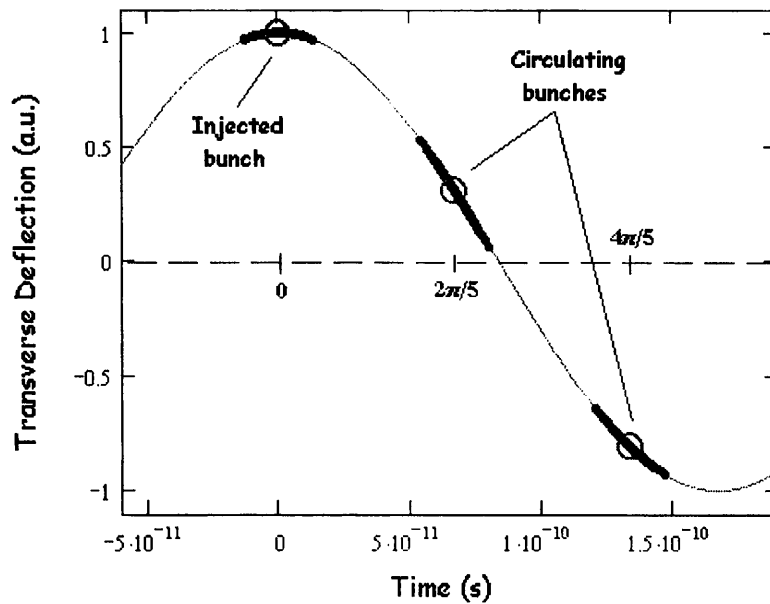
Figure 4.17: Kick amplitude for injected and circulating bunches

As a consequence of the phase extension, the head and the tail of the circulating bunches experience different deflection angles. This enlarges the transverse size of the circulating beam in the region between the two RF deflectors. This effect represents the dominant contribution to the beam size at the level of the septum. The main constraints on the size of the beam are the limit of the vacuum chamber and the thickness of the septum in the chamber. In order to limit the

phase extension, short bunches are essential, and simulations have shown that the maximum acceptable bunch length is around 15 ps FWHM for a combination factor of five.

The simplest injection process makes use of the RF deflectors only. However, it is also possible to use a combination of bumpers and RF deflectors. Indeed, to provide a significant reduction of the angular deflection needed from the RF deflectors, bumpers are also located close to the deflectors and can be used to add a static closed bump to the time-dependent bump of the deflectors.

Figure 4.18 shows the envelopes of Gaussian bunches of length 10 ps FWHM (truncated longitudinally at $\pm 2\sigma$ with a 2σ extension in the transverse plane) in the injection region in the case of RF deflectors only. The deflection angle on the crest is the reference value 4.5 mrad. In this case, the circulating beam is deflected to the opposite side of the septum. On the other hand, Figure 4.19 illustrates the situation when the bumpers and the deflectors are used together. The deflection angle for the deflectors is 2.5 mrad on crest, and the angle in the bumpers is 2 mrad. In this case, the beam envelopes are shifted closer to the septum. Both methods seem experimentally feasible and provide some flexibility in operation.
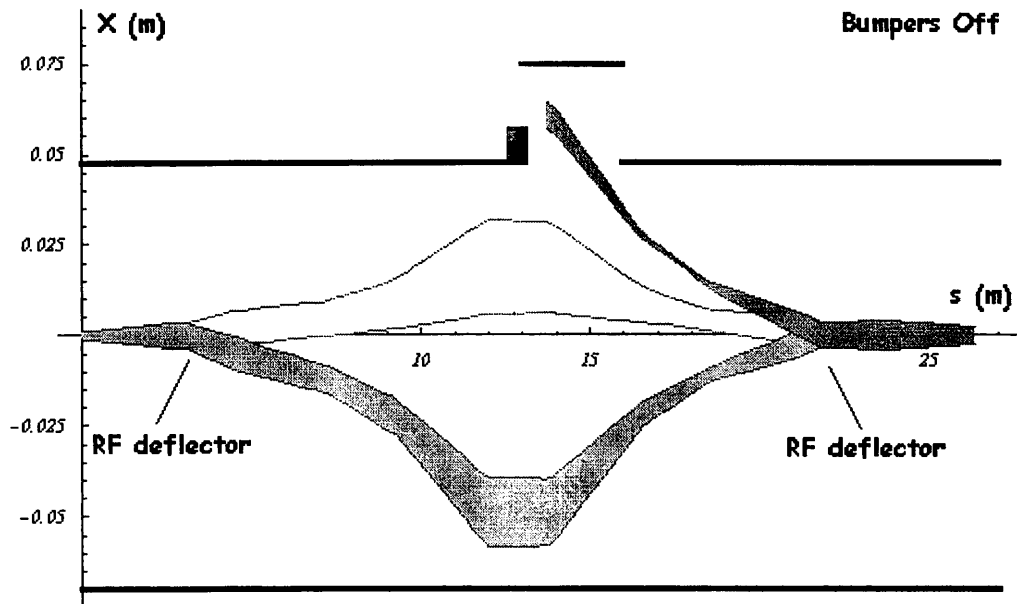
Figure 4.18: Beam envelopes of injected and circulating beams in the RF deflectors.
(Bumpers off)
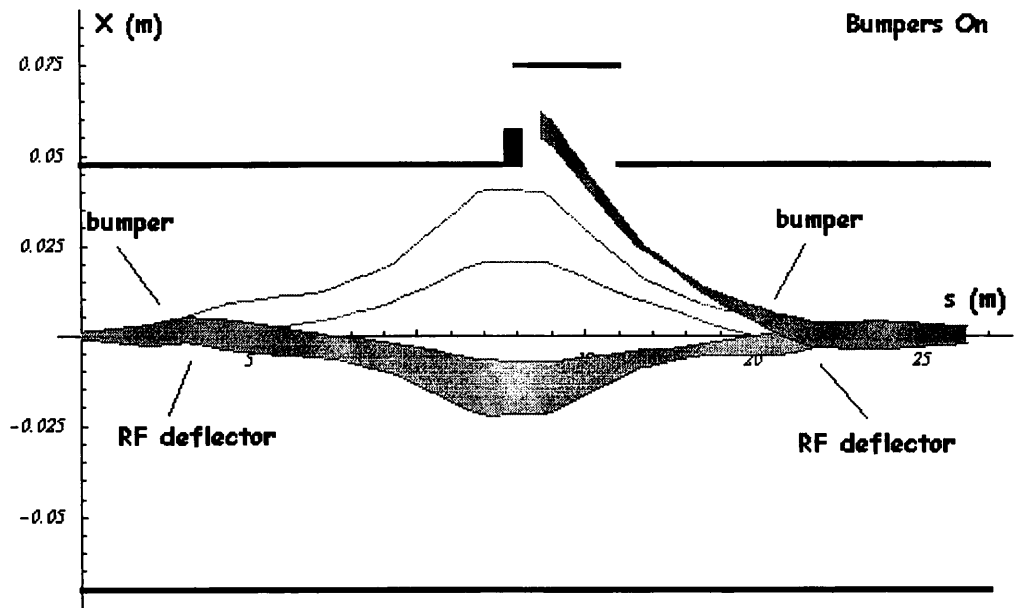
Figure 4.19: Beam envelopes of injected and circulating beams in the RF deflectors.
(Bumpers on)

4.8 Complete tracking in the transfer line and in EPA

In order to check that the optics satisfies the requirements, a complete tracking through the modified transfer line and the isochronous ring has been carried out. Such a tracking allows to take into account the higher order effects in chromaticity and isochronicity in a global way. For this purpose, new tracking routines have been written on the basis of the MAD program, to generate realistic distributions of particles [1]. The results of the tracking in the transfer line and the new EPA ring are presented in Figure 4.20.
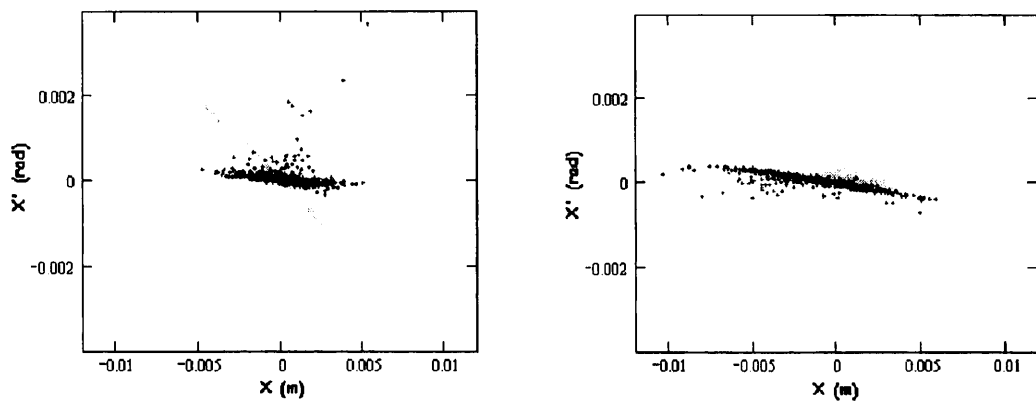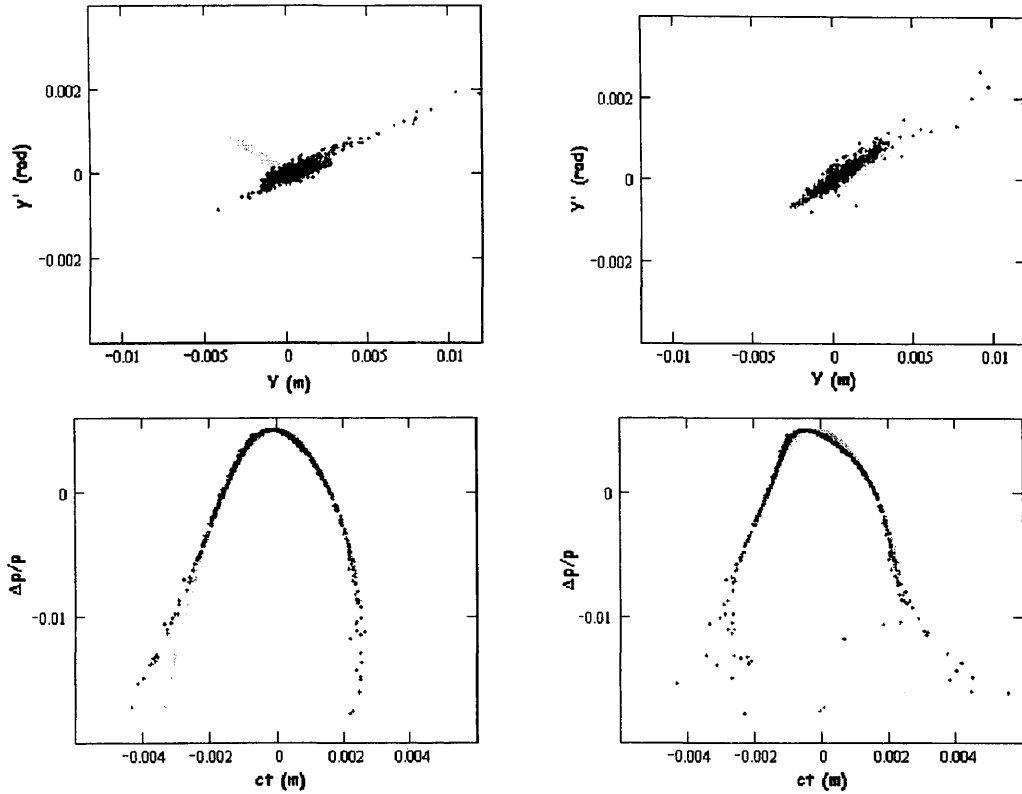
Figure 4.20: Tracking in the transverse and longitudinal planes in the transfer line (left) and in the isochronous ring after five turns (right)

Tracking has also been performed through the matching section at the end of the linac, where no important aberration effects have been found. For all simulations, a 6-D Gaussian particle distribution was generated, with a bunch length of 10 ps FWHM (or 1.28 mm rms), and a normalised rms emittance of 40 π mm mrad in both transverse planes. The longitudinal phase space at the entrance of the matching section has been calculated taking into account the phase extension of the bunch with respect to the accelerating RF field, for a final energy at the end of the linac of 350 MeV.

The left-hand side of the figure shows the tracking in the transfer line. The initial phase space is derived from the values of the Twiss parameters at the end of the linac (point zero), assuming a perfect matching between the linac and the transfer line. The final distributions result from one passage through the line. The right-hand side of the figure shows the tracking in the isochronous EPA ring. The initial distributions are the result from the tracking in the transfer line taken at the injection point, and the final distributions are given at the same point, after five turns in the ring. The difference between the initial and final transverse distributions indicate a small mismatch at the entrance to the ring. However, the discrepancy remains small. On the other hand, the longitudinal tracking shows no bunch lengthening. Less than 1% of the particles are lost after the tracking over five turns, mainly in the tails of the distributions. The tracking has been extended to 100 turns in the ring, which shows that the losses are kept at a low level (around 1.5%) and occur only in the first turns, which confirms the stability of the solution.

4.9 Extraction Line

A new extraction line is implemented in the former e⁺ injection line. The kicker (KFE11) and the septum (SMH33) used to inject positrons into EPA will be used to extract electrons from EPA. The electron beam is sent towards a dump. Just upstream of the dump, a new scintillator screen (HEE.MTV04) and a new Beam Position Monitor (HEE.UMA04) will be installed.

4.10 Beam steering

Beam Position Monitors (UMAs) and correction magnets from the existing LPI complex will be used. UMAs are installed in the front-end, the linac, the transfer lines and EPA. Small trim dipoles are distributed in the present installation, and a number of quadrupole magnets have separate windings that serve as correction dipoles. Figure 4.21 shows the phase advance along the linac together with the monitor and corrector locations for both the horizontal and the vertical planes. It can be seen that the phase differences between the monitors are sufficiently small to sample the trajectory well. The distribution of the correction dipoles is also suitable for trajectory correction.
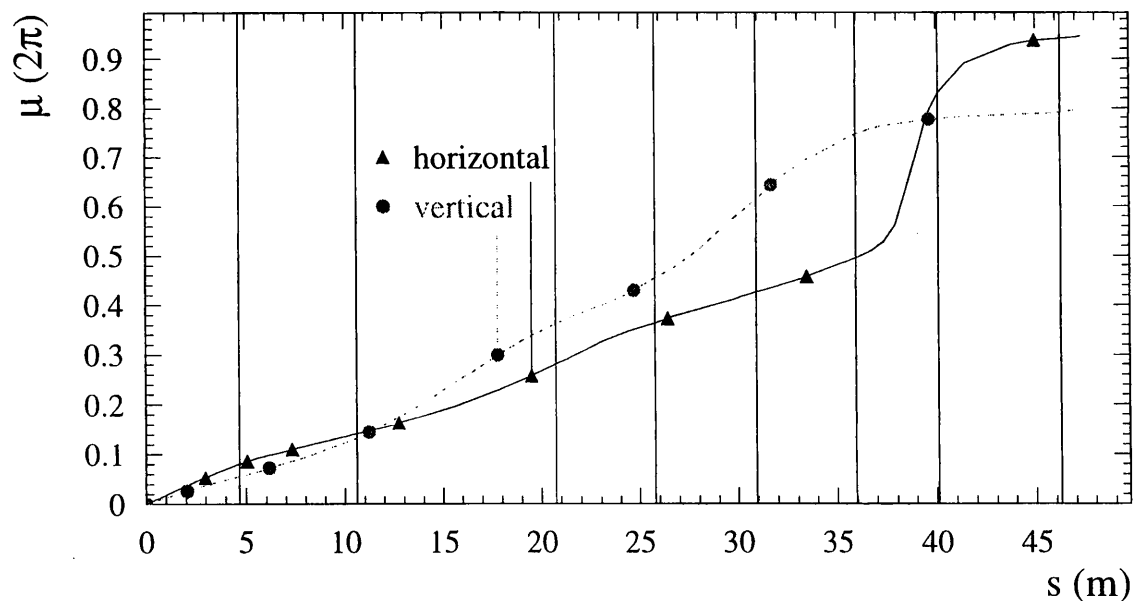
Figure 4.21: Phase advance along linac with positions of UMAs (indicated as vertical lines) and corrector locations (markers)

The 19 existing UMAs in the EPA ring are sufficient to ensure a good injection optimisation and trajectory correction (the tunes are $Q_x \cong 4.73$ and $Q_y \cong 3.77$). The present ring has only two correction dipoles per transverse direction, but additional correctors might be added to ease operation and to avoid the displacement of quadrupoles for trajectory correction.

It is foreseen to implement automated beam steering (ABS) for the linac, the injection line and the ring. This will be done in the framework of the general PS ABS project [14] with a description of the machine in the accelerator database [15].

4.11 Beam Diagnostics Considerations

The essential aspects are related to the reorganisation of the existing LPI complex as described above, i.e. the shortening of LIL, modification of the EPA ring lattice, etc. The existing diagnostics systems need to be relocated and adapted to the new parameters where necessary. Most beam diagnostics tools required are already described above.

For the beam position monitoring, the existing devices in LIL and EPA will be kept as they are, they will, however, be moved to new positions where necessary. Redundant devices from the existing complex will be disconnected. It is foreseen to modify the software to permit controllable and appropriate positioning of the integration gate as well as to control the gain of the amplifiers. To study the beam optics of the isochronous EPA ring, it is foreseen to use the discrete output of the delta signals in both planes from UMA41 (zero dispersion region) and UMA53 (finite dispersion region) over several turns ($\leq$ 1000) with appropriate sampling devices in the control system.

The Wire Beam Scanners, SEM grids and scintillator screens will be re-used and moved to new positions wherever necessary. Image frame grabbing systems and digital treatment will be implemented where appropriate to complement visual images from screens.

A streak camera, recuperated from the LEP ring will be installed in the synchrotron radiation laboratory outside the EPA ring and will be used for beam studies in LIL and EPA. It will use existing synchrotron light ports MSR52, MSR56 and MSR58. Since MSR58 was used for positrons in the past its vacuum section must be modified to permit rotation of the copper mirrors in the right direction for electrons. The existing light guides, the precision rail on the ceiling, achromat lenses and pellicle beam splitters will be verified for light transport to the streak camera. Two Transition Cerenkov Monitors TCM36 and TCM37 will be installed in the new matching section between LIL and the Injection Line feeding the modified EPA Ring. These will be used in conjunction with the streak camera. The light transport system from these two TCMs will be installed such that no additional holes in the shielding are necessary. This permits linking the TCMs' light channels to the refurbished channels of MSRs mentioned above, with the addition of a few rotating and controllable mirrors.

Wall Current Monitors will be used for measuring the beam current.

The preliminary phase for CTF3 will be used as a test bed for new techniques and diagnostics tools required for the later phases of the project.

4.12 Control System

The controls for CTF3 will re-use the infrastructure in place for LPI and CTF2. However, this infrastructure must be upgraded and re-organised before being extended for the different phases of the CT3 project. The LPI to CTF3 transformation described in the previous paragraphs will require many modifications and extensions to the LPI control system for the preliminary phase, but only points requiring new development are described here. One of these is the timing system, which is described in chapter 4.13

4.12.1 Upgrade of the LPI Controls Infrastructure

The control system of the LPI follows the current standard of the PS control system and is composed of VME-based front-end computers and Unix workstations. The front-end computers are named DSC (Device Stub Controller) and use the real-time operating system LynxOS. The

control system was upgraded in 1991. However, a big part of the control interfaces implemented during the LPI construction, based on CAMAC has been maintained.

Because of the planned demise of the LPI machine, its control system has not been upgraded to the same level as the other machines of the PS Complex. The upgrades that need to be made during the preliminary phase are the following:

a) Installation of Ethernet structured cabling.

b) Replacement of the VME 68040-based CPU with the PowerPC-based version.

c) Replacement of the CAMAC-based timing distribution with the VME-based MTG/TG8 system

d) Phasing-out of obsolete CAMAC modules that cannot be maintained for 5 more years.

e) Replacement of the IBM/AIX workstation with new PC/Linux (control room).

4.12.2 Re-organisation of the LPI controls layout

A total of 17 DSCs were used for LPI (12) and CTF2 (5). These DSCs control 39 CAMAC crates. The number of DSCs used for the preliminary phase will remain about the same (~20). However, the control layout needs to be modified for the following reasons:

- The new CPU have different characteristics: three different DSCs were used for the control of the LPI modulators, which are no longer required.

- A big part of the inter-building cabling, done during the LPI construction, should not be extended and can even be reduced by re-distributing the front-end computers. This is motivated by reducing the cabling costs and improving the reliability.

- We must constrain the CTF3 exploitation cost by rationalising the control layout. Otherwise, we will face priority conflicts with the support for the other six accelerators of the PS Complex. In particular, we aim at suppressing as far as possible intermediate CAMAC interfaces between DSCs and local electronics (e.g. G64-based power supply control). This concerns, for example, more than 100 power supplies.

- The machine extension during the next phases must be taken into account. This implies, for instance, moving the fibre-optic star point from the klystron gallery to building 2013.

4.12.3 Integration of PLC-controlled equipment

The integration of PLC-controlled equipment into the PS control system is an extension that is currently prepared by the PS/CO group and will be extensively used in the framework of the ISOLDE renovation.

This extension must be deployed in CTF3 in 2001 for the new modulator used for the RF deflectors. The introduction of PLCs for local controls is an important trend that is supported by the PS/CO group. The MDK33 control is one of the first applications of this approach in the complex and it represents a major improvement in the way such complex devices can be controlled, especially for the interlock management, the start-up sequence execution and the local interaction.

4.12.4 Support for PCI-based front-end computers

The streak-camera described in chapter 4.11 will use a PCI frame-grabber. A PC/Linux front-end will be used for this device. It will be the first operational front-end of this kind in the PS control system.

The PS control software (LynxOS) will be ported to this environment (Linux) and the streak camera is a pilot project for building a new category of front-end computers, based on a PC architecture and on Linux, that will complement our VME-LynxOS systems in similar cases on other accelerators.

4.13 Timing for CTF3 Preliminary Phase

As much as possible of the present LPI timing system will be used for the preliminary phase of CTF3. This includes the system for generating the 19 MHz train synchronised to the 50 Hz network zero-crossings, as well as the 19 MHz CAMAC programmable counters which produce the timing pulses for the gun, klystrons etc. However, in the present scheme, there is no synchronisation between the 19 MHz and the 3 GHz of LIL. For demonstrating bunch combination in EPA, the gun timing as well as a streak camera trigger should be synchronised to the 3 GHz. New hardware will be developed to achieve this. In addition, some changes are required to the machine timing system.

4.13.1 Modification to the Central Timing

4.13.1.1 De-coupling from PS

The central Master Timing Generator (MTG), which provides the timing for the PS Complex, uses a beam description which locates the relative times of the cycles in different accelerators according to injection and ejection rendezvous points, where the beam is transferred between machines. The current LPI accelerator has lepton transfer rendezvous with the PS accelerator, and hence it has a super-cycle, cycles for electrons or positrons, and is controlled by the LPI telegram which pilots the PS standard PPM (Pulse-to-Pulse Modulation) mechanism, real time tasks, and application programs.

Suppressing the LPI telegram completely, even if there were no CTF3, would be a very big job as it involves deleting the LPI machine from the Oracle database and consequently rebuilding almost the entire PS Complex control system.

The CTF3 will not be strongly coupled to the PS machine, although there may be some second order reasons for doing so, such as avoiding undesirable side effects from electrical noise, or other factors effecting repeatability. The CTF3 may also need to tag acquisition data with a basic period number, or perhaps a universal time stamp as in other machines and, having acquired the data, it must store them somewhere where they can later be accessed by application programs. Some slow timing will be needed to co-ordinate this activity, especially if correlation of data from physically separate processes is to be achieved.

The CTF3 will also need to control the production or dummy timing selection currently piloted by a real-time task in a controller, termed the IKBOX, via the LPI telegram.

For these reasons the telegram concept would still seem to be relevant to the CTF3 machine, and the 1.2 s and 1 kHz trains defining the coarse timing and the Basic Period will also be needed. Building a CTF3 super-cycle is, however, completely irrelevant.

We propose to leave the LPI telegram in place, and create the alias "CTF" by which it can be referenced. The structure of the CTF telegram will include "groups" i.e. parameters controlling production/dummy timing selection, the EPA bucket filling scheme, 3 GHz synchronised RF or not (see section 2), and acquisition tags. We propose to declare the CTF machine as "loosely-coupled" to the MTG, suppressing completely the idea of super-cycle and to

pilot the data in the CTF telegram via MTG equipment calls and external conditions. This requires some modifications to the PLS-Editor application program, to the MTG volatile logic (FIDO), and to the super-cycle update process. This work is estimated very roughly as about one man month of effort.

4.13.1 .2 IKBox clean-up

There are currently 120 declared timings for the IKBOX controlled from the DSC DLPITIMG. Those not required for CTF3 have been identified and will be removed.

4.13.1 .3 Zero-point crossing synchronisation

The 1 KHz frequency of the coarse timing system will be synchronised to the 100 Hz of the mains network. Many of these timings can be suppressed completely, and others derived directly from the MTG. This will be better understood when we have a clear idea about how the CTF3 will be operated.

4.13.1 .4 Suppression of old serial telegram

The old style telegram will be replaced by the new CTF telegram, distributed over the MTG timing drop net for the Tg8s. Today the LPI telegram pilots the production/dummy mode, and it must be distributed synchronously with the linac period to avoid jitter between the C-train and the 100 Hz, which would result in losses in control of the first linac period in a Basic Period.

4.13.2 RF Synchronisation

At present, there is no synchronisation between the 3 GHz LIL and 19 MHz EPA RF systems. All digital delays (for gun, klystrons etc.) are derived from the EPA frequency. A simplified layout is shown in Figure 4.22. A 3 ms train of 19 MHz pulses is generated, synchronised to the 50 Hz network zero-crossing, and the first pulse is selectable to fill the required EPA bucket. This train is then sent to the GPPC CAMAC counters, which generate the timing pulses.
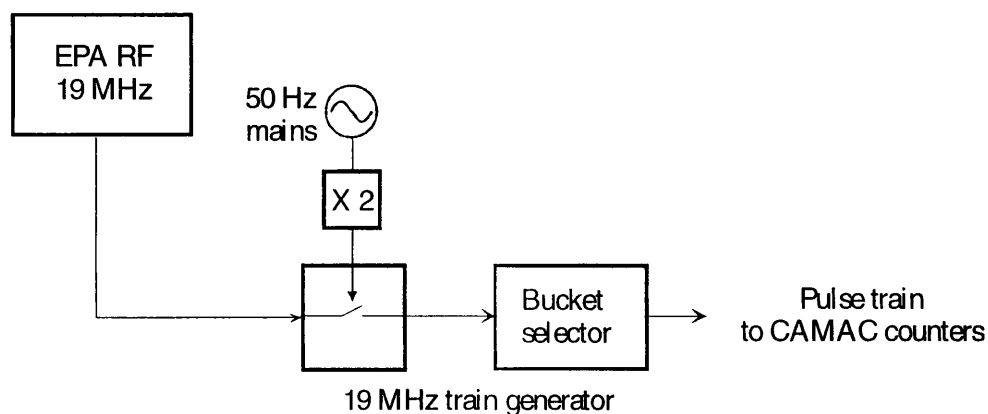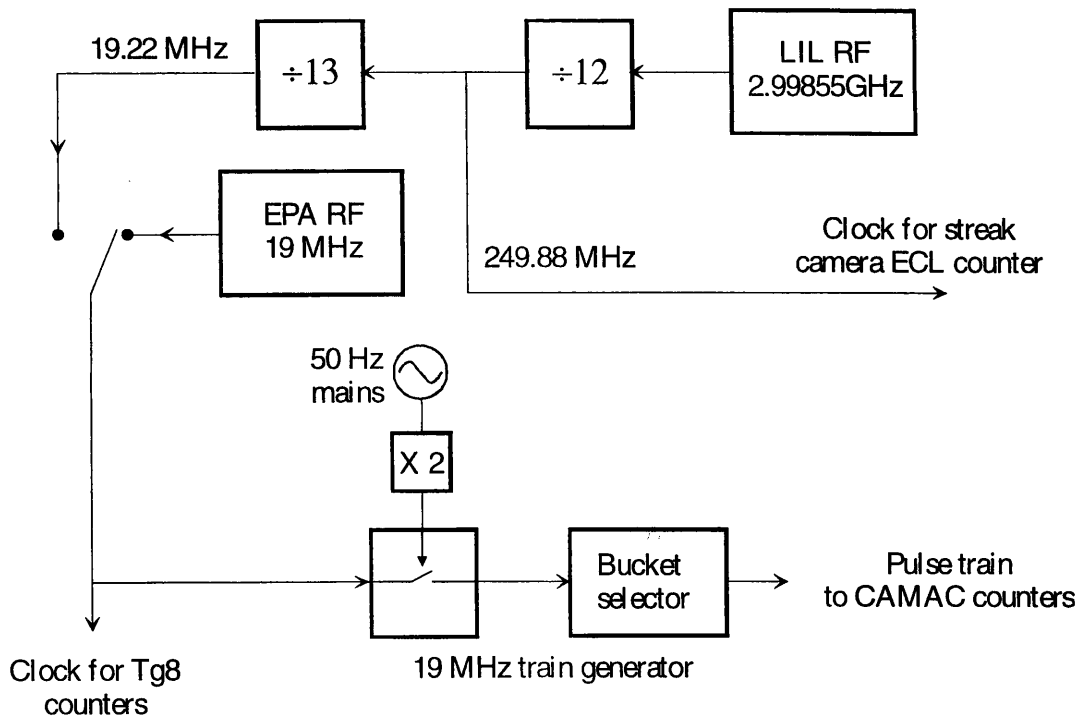

19 MHz train generator

Figure 4.22: Current LIL 19 MHz timing (simplified).

36

Figure 4.23: Proposed synchronisation for CTF3 preliminary phase (simplified).

This scheme is not suitable for CTF3 running for the "recombination" mode. The gun and the streak camera must be synchronised to the 3 GHz. To solve this problem, two running modes are proposed, with and without 3 GHz synchronisation (Figure 4.23). In "Accumulation mode" there will be no 3 GHz synchronisation. The two RFs will be independent and the timing will essentially be as for LIL. When testing recombination in EPA, the RF cavity will be switched off and the timing switched to a 19.2 MHz signal derived from the 3 GHz. Due to the slight frequency difference, two sets of data will be required for loading into the CAMAC counters. Division of the 3 GHz will be in two stages. The 250 MHz will be used as a clock for the streak camera trigger counter. The 3 GHz divider chain requires development.

4.13.3 Digital Delays

4.13.3.1 Existing LIL equipment

Timing pulses are presently generated by GPPC CAMAC modules. These and their associated blocking level drivers will remain in use for the preliminary phase of CTF3 for all existing equipment. At a later stage, it is planned to replace them by Tg8 counters or (wherever precision necessitates) especially developed ECL (emitter-coupled logic) counters. The drivers will also be replaced. This electronics, which is currently under development, will be used exclusively for new timing requirements for the preliminary phase (i.e. gun and streak camera).

4.13.3 .2 Gun timing

The gun requires two timing signals:

- A start pulse, of approximately 50 ns pulse width.

- A train of pulses with a spacing of 420 ns, adjustable to better than 0.5 ns. There will be a maximum of seven pulses, with the possibility to independently enable or disable each one. The pulse width should be about 50 ns. It need not be variable, as the timing does not control output pulse length. Both signals should be 50 Ω TTL.

It is proposed to implement these signals using the newly modified PS Tg8 standard. These modules incorporate counters that can be clocked at 19 MHz (Figure 4.24). Resolution will be improved to 0.2 ns by the addition of an Analog Devices AD9501 delay chip at the output. Unlike the GPPC CAMAC modules, these counters will have a continuous clock input with counting enabled by a start pulse. This will facilitate clock distribution later on and corresponds to the architecture of the ECL counters described below.

As is currently the case for the IKBOX, all timings will be generated in parallel, and selected by placing a logic 1 level on the select gate. The select lines can be driven by a standard telegram driven real-time task controlling a digital output VME module (VMOD DOR) each linac period (100Hz).

4.13.3 .3 Streak camera timing

The streak camera requires a trigger with a short-term stability of better than 10 ps. An ECL delay card capable of this is being developed. It will be clocked at 250 MHz and have a vernier delay resolution of 20 ps. This card, which is being developed for multiple uses for the CTF3 nominal phase, will not be completed for 2001. However, for the streak camera, a prototype will be available. The ECL counter will receive its start trigger from a Tg8 19 MHz counter output.

4.13.3 .4 Line drivers

For distribution of the gun and streak camera timing signals, new 50 Ω line drivers are being developed. They will be able to provide a pulse up to 10 V with a rise time of the order of 1 ns. It is planned to use these drivers extensively in the later stages of CTF3. They will replace the blocking level drivers that, due to their slow rise-times, give excessive timing uncertainty.
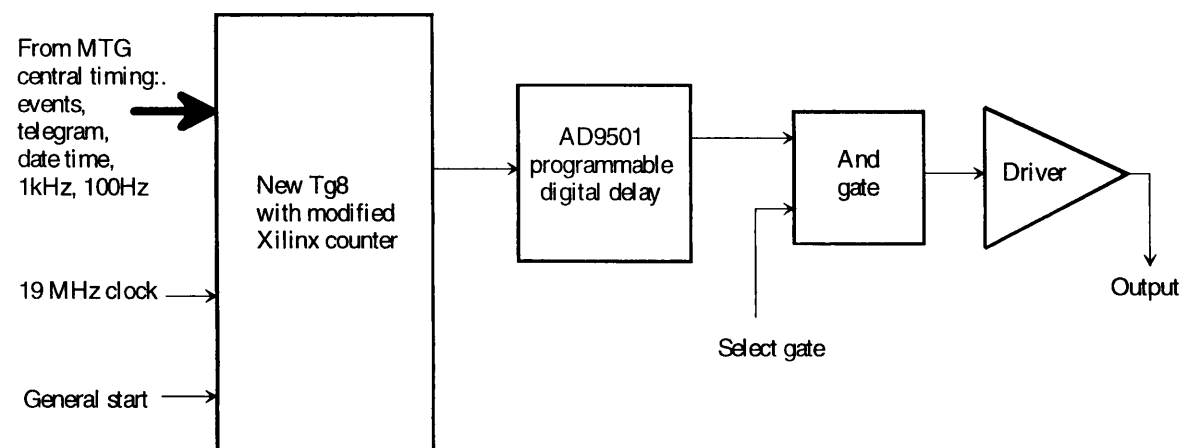

Figure 4.24: General purpose Tg8 timing channel

5. SCHEDULE AND EXPERIMENTAL PROGRAMME

The final goal of the Preliminary Phase of CTF3 is to perform a low-charge, short pulse demonstration of the concept of bunch train combination by RF deflectors in an isochronous ring, covering a range of combination factors from three to five. It will also give the opportunity to acquire experience in combiner ring operation, to develop techniques and tools and to test hardware in preparation for the next phases.

The experimental program extends over 2001 and 2002. The scheduled operational time with beam is about six weeks at the end of 2001 and for a maximum of 20 weeks in 2002. The hardware modifications to the present LPI installation will be made during the shut-down from April 17th 2001 to September 17th 2001. A first commissioning run will start as soon as the hardware modification are completed and will continue until December 14th. The 2002 running period will coincide with the normal operating period of the PS Complex, starting after the winter shut-down.

During commissioning, we will typically run with beam for two weeks, then stop for about the same period. Running for longer periods without interruption is not compatible with the manpower available for operation. The regular down-time periods will also allow us to analyse the measurements, to prepare the subsequent experiments, and will be used for maintenance and hardware interventions. It must be noted that if some non-vital components are not ready for installation before the scheduled start-up date, these periods would allow completion of the installation without affecting the experimental programme.

The goal of the 2001 run is the commissioning of the new installation (front-end, linac, matching/diagnostics section, injection line, ring and extraction). A first series of measurements will be made in order to ensure that the hardware works as expected and to check and calibrate the beam diagnostic systems. The beam will then be fully characterised using the diagnostics section at the end of the linac, and the front-end/linac optics will be optimised. The injection line and the ring will then be put into operation. In the 2001 run, the RF deflectors will not be installed (only a temporary installation is planned at the end of the shutdown to check the mechanical assembly). Therefore, injection will be done using the conventional kickers. Two different modes of operation are foreseen:

a) *Accumulation mode*: a new optics with a relatively large momentum compaction ($\alpha \sim 10^{-2}$) will allow to store the beam and will mainly be used to perform ring optics measurements (tunes, chromaticity, closed orbit). This mode of operation will make it easier to validate the machine model (MAD simulations) in the new configuration with lower beam energies.

b) *Recombination mode*: the isochronous optics (zero momentum compaction) will be used with axial injection (no beam accumulation). In this mode of operation, measurements of the beam properties at injection into the ring will be made to optimise and match the injection line optics to the ring. Streak camera measurements of the synchrotron radiation will be used to check the isochronicity of the system and to minimise the bunch length after injection.

During the 2001 run, the gun will be used mainly in single-pulse mode, however, during the linac commissioning the multi-bunch mode will be tested, and beam-loading measurements performed in order to assess the upper limit for the total charge.

The RF deflectors will be installed in the ring in 2002. At first, the single-pulse mode will be used and the injection process with RF deflectors will be optimised for the different combination factors. Only then will multi-pulse operation start, and studies of the real

combination process. The streak camera with synchrotron radiation will be the main instrument used to demonstrate the combination.

Further experiments could be made, depending on the time and resources available. These include measurements of the effect of the ring impedance and coherent synchrotron radiation on the beam and of transverse stability of the beam in the RF deflectors. A pair of large aperture (~ 40 mm) prototypes of RF deflectors presently under development in INFN-Frascati might become available at the beginning of 2002. They could replace the existing ones which have a smaller aperture.

6. REFERENCES

[1]   R. Corsini, A. Ferrari, L. Rinolfi, T. Risselada, P. Royer, F. Tecker, "Beam dynamics for the CTF3 preliminary phase", CLIC Note 470, January 2001.

[2]   R. Corsini, J.P. Potier, L. Rinolfi, T. Risselada, "Isochronous optics and related measurements in EPA", Proceedings of the 7th European Particle Accelerators Conference, Wien, June 2000.

[3]   R. Chaput, "Electron gun for the FEL CLIO", Proceedings of the 2nd EPAC Conference, Nice, 1990.

[4]   J.C. Bourdon, R. Belbeoch, M. Bernard, P. Brunet, B. Leblond, M. Omeich, E. Plouviez, J. Rodier, "Commissioning the CLIO injection system", Nuclear Instruments Methods in Physics Research A304, 322-328 (1991).

[6]   H. Grote and F.Ch. Iselin, "The MAD Program", CERN/SL/90-13(AP), Rev.3,(1993).

[7]   K.L. Brown, D.C. Carey, F.Ch. Iselin and F. Rothacker, "TRANSPORT-A Computer Program for Designing Charged Particle Beam Transport Systems", CERN 80-4, (1980).

[7]   A. Pisent, L. Rinolfi, "A new bunching system for the LEP Injector Linac", CERN/PS/90-58 (LP).

[8]   R. Corsini, A. Ferrari, L. Rinolfi, T. Risselada, P. Royer, F. Tecker, "New measurements of the LIL bunch length and lattice parameters", CTF3 Note 2000-13 (MD-LPI) and PS/LP Note 2000-02 (MD).

[9]   R. Corsini, J.P. Potier, L. Rinolfi, T. Risselada, J.C. Thomi, "First micro-bunch measurement in EPA as isochronous ring at 500 MeV", PS/LP Note 99-03 (MD).

[10]   R. Corsini, B. Dupuy, A. Ferrari, L. Rinolfi, T. Risselada, P. Royer, F. Tecker, "LIL lattice parameters, LIL energy gains, LIL temperature versus frequency, EPA circumference and EPA isochronicity measurements", CTF3 Note 2000-18 (MD).

[11]   R. Belbeoch, "Pouvoir de résolution dans la mesure de la distribution longitudinale des paquets à la sortie du groupeur du linac pre-injecteur de LEP", LAL PI 85-06/T, Orsay, Avril 1986.

[12]   P. Bernard, H. Lengeler, V. Vaghin, "On the design of disk-loaded waveguides for RF separators", CERN 68-30 (1968).

[13]   D. Alesini, R. Boni, A. Gallo, F. Marcellini, "The RF deflectors for CTF3", Frascati Note CTFF3-003, April 2001.

[14]   B. Autin, F. Di Maio, M. Gourber-Pace, M. Lindroos, J. Schinzel, "Data base for accelerator optics", CERN/PS 97-065, International Conference on Accelerator and Large experimental physics control systems, 3-5 November 1997, Beijing, China.

[15]   L. Rinolfi, J. Schinzel, "CTF3 project information management proposal", CTF3 Note 2000-017 (EDMS).

41

7. APPENDICES

7.1 Appendix 1

Central positions (with respect to the entrance of ACS27) and properties of the quadrupoles in the linac and in the matching section. Positive (respectively negative) currents and normalized gradients stand for focusing (respectively defocusing) quadrupoles. The beam energy is 4~MeV at the beginning of the linac and 350~MeV at the end of the linac, i.e. in the matching section.

Name	Length (mm)	Current (A)	K (m^{-2})	Distance (m)
WL.QNM271	328	0	0	0.321
WL.QNM272	328	0	0	0.801
WL.QNM273	328	0	0	1.824
WL.QNF271	328	0	0	2.304
WL.QNF272	328	0	0	3.010
WL.QNF273	328	0	0	3.635
WL.QNF274	328	0	0	4.232
WL.QLB28	220	0	0	5.031
WL.QNF281	328	0	0	5.767
WL.QNF282	328	0	0	6.581
WL.QNF283	328	0	0	7.451
WL.QNF284	328	0	0	8.381
WL.QNF285	328	0	0	9.374
WL.QLB29	220	-5.0	-0.926	10.446
WL.QNF291	328	+20.0	+0.996	11.541
WL.QNF292	328	-20.0	-0.894	12.712
WL.QNF293	328	+20.0	+0.806	13.946
WL.QNF294	328	-20.0	-0.734	15.182
WL.QNF301	328	+20.0	+0.686	16.626
WL.QNF302	328	-20.0	-0.623	18.126
WL.QNF303	328	+20.0	+0.567	19.732
WL.QNF311	328	-20.0	-0.532	21.457
WL.QNF312	328	+20.0	+0.488	23.184
WL.QNF313	328	-20.0	-0.450	24.914
WL.QNF321	328	+20.0	+0.428	26.644
WL.QNF322	328	-50.0	-0.976	28.374
WL.QNF323	328	+50.0	+0.914	30.104
WL.QNF331	328	-50.0	-0.874	31.834
WL.QNF332	328	+50.0	+0.823	33.564
WL.QNF333	328	-50.0	-0.778	35.304
WL.QNF341	328	+50.0	+0.751	37.064
WL.QNF342	328	-50.0	-0.712	38.864
WL.QNF343	328	+50.0	+0.676	40.692
WL.QNF351	328	+70.0	+0.960	42.174
WL.QNF352	328	-72.7	-0.997	43.302
WL.QNF361	328	+54.6	+0.749	45.030
WL.QNF362	328	-162.9	-2.233	50.344
WL.QNM363	328	+198.1	+2.716	51.172
Point zero	-	-	-	51.636

7.2 Appendix 2

Central positions (with respect to point zero) and properties of the magnetic elements in the new transfer line for the CTF3 preliminary phase. Positive (respectively negative) gradients stand for focusing (respectively defocusing) quadrupoles.

Element	Angle (degrees)	Gradient	Position
HIE.BSH00	-9		1.077 (unchanged)
HIE.BVT00	+0.55(vertical)		2.526 (unchanged)
HIE.QFW01		+4.360	3.263 (new)
HIE.BHZ10	-20		4.474 (unchanged)
HIE.QDW11		-4.360	5.578 (unchanged)
HIE.BHZ20	-20		6.724 (unchanged)
HIE.QFW21		+2.870	8.383 (moved)
HIE.QDW22		-2.948	9.258 (moved)
HIE.QFW23		+2.154	12.649 (moved)
HIE.QDW24		-3.040	13.975 (moved)
HIE.QFW25		+3.712	15.450 (unchanged)
HIE.BHZ30	+20		16.270 (unchanged)
HIE.QFW30		+3.980	17.291 (new)
HIE.BVT30	-0.55(vertical)		17.918 (unchanged)
HIE.SMH31	+21.75		18.916 (unchanged)
HIE.SMH32	+7.25		19.619 (unchanged)

7.3 Appendix 3

Normalized gradients of the quadrupoles and sextupoles (XNH and XNV) for the EPA isochronous optics. Positive (respectively negative) gradients stand for focusing (respectively defocusing) quadrupoles.

Quadrupole Name	length (m)	current (A)	Normalized gradient (m^{-2})
HR.QFWa	0.380	33.0	+1.017
HR.QFWb	0.380	18.8	+0.581
HR.QFLa	0.380	96.8	+2.566
HR.QFLb	0.380	11.4	+0.305
HR.QTRa	0.358	7.2	+0.176
HR.QTRb	0.358	44.5	+1.084
HR.QFN	0.358	23.3	+0.566
HR.QDN	0.358	-23.4	-0.569
HR.QFI	0.380	19.9	+0.534
XNH	0.246	16.5	7.008
XNVa	0.246	81.8	34.724
XNVb	0.246	56.6	24.027

7.4 Appendix 4

Normalized gradients of the quadrupoles and sextupoles (X...) for the EPA non-isochronous optics. Positive (respectively negative) gradients stand for focusing (respectively defocusing) quadrupoles.

Quadrupole Name	length (m)	current (A)	Normalized gradient (m^{-2})
HR.QFWa	0.380	47.9	1.475
HR.QFWb	0.380	20.7	0.638
HR.QFLa	0.380	96.4	2.555
HR.QFLb	0.380	-47.5	-1.260
HR.QTRa	0.358	-11.3	-0.276
HR.QTRb	0.358	42.8	1.041
HR.QFN	0.358	23.7	0.566
HR.QDN	0.358	-23.4	-0.569
HR.QFI	0.380	19.9	0.534
XNH	0.246	9.8	4.19
XNVa	0.246	-28.7	-12.18
XNVb	0.246	58.4	24.78